GROWTH OF MECHANICAL TWINS IN ZINC SINGLE CRYSTALS

Thesis for the Degree of Ph. D.

MICHIGAN STATE UNIVERSITY

Man Hyong Yoo

1965

This is to certify that the

thesis entitled

GROWTH OF MECHANICAL TWINS
IN ZINC SINGLE CRYSTALS

presented by

Man Hyong Yoo

has been accepted towards fulfillment
of the requirements for

Ph. D. degree in Metallurgy

Major professor

Date December 14, 1965

ABSTRACT

GROWTH OF MECHANICAL TWINS
IN ZINC SINGLE CRYSTALS

by Man Hyong Yoo

The growth process of the $\{10\bar{1}2\}\ <10\bar{1}\bar{1}>$ type twin in hexagonal close-packed zinc crystals is investigated from the geometric and the energetic points of view. A mechanism for the twin growth by the incorporation of slip dislocations at the coherent twin boundary is proposed. The geometric aspect of the incorporation process has been analyzed by using matrix algebra, whereas the energetic factors have been calculated by applying anisotropic elasticity theory of dislocations. Experimental observations on the process of twin growth do not in any way contradict the proposed mechanism.

Based on the anisotropic elasticity calculations, the interaction of a pair of twin dislocations in the edge orientation has been derived from the stress field of such a twin dislocation and found to be in general noncentrosymmetrical. Three possible shapes of advancing twin interfaces can be predicted in accordance with the stable configurations of a group of twin dislocations; of these three two have been observed. The energy associated with the coherent twin boundary is estimated to be 1.4 ± 0.4 ergs/cm^2. The results of calculations of the elastic energies of the various slip dislocations are applied to a discussion of the feasibility of certain dislocation dissociation processes.

GROWTH OF MECHANICAL TWINS IN ZINC SINGLE CRYSTALS

By

Man Hyong Yoo

A THESIS

Submitted to
Michigan State University
in partial fulfillment of the requirements
for the degree of

DOCTOR OF PHILOSOPHY

Department of Metallurgy,
Mechanics and Materials Science

1965

ACKNOWLEDGEMENTS

The author wishes to express his gratitude to Professor C. T. Wei for his aid during the course of this study. He sincerely thanks him also for his encouragement and guidance extended throughout the entire graduate program. He is indebted to the other members of his graduate committee, Professors A. J. Smith, L. E. Malvern, and D. J. Montgomery.

Special thanks are due to the members of his family for their patient cooperations. He is grateful to Mr. J. W. Hoffman and the Division of Engineering Research for continuous support. This study has been made possible through a grant from the National Science Foundation, G-19652.

TABLE OF CONTENTS

Table of Contents -- (continued)

LIST OF TABLES

LIST OF FIGURES

LIST OF APPENDICES

by wh

defor

theor

well

of th

clear

are

thre

crite

crys

twin

mec

deve

the

mu

ma

Th

tw

by

I. INTRODUCTION

Mechanical twinning is one of the two fundamental processes by which crystalline solids can be plastically deformed. The other deformation process, namely slip, has been extensively studied both theoretically and experimentally, and consequently it is in general well understood. On the other hand, except for the crystallography of the twinned structures, the process of mechanical twinning is not clearly understood as far as the nucleation and the growth of twins are concerned. In order to understand a mechanical twinning process three aspects of the twinning process are to be investigated: 1) the criteria that a particular twin system should be operative and its crystallography, 2) the nucleation of twins, and 3) the growth of twins. As a part of a research project for the investigation of the mechanical twinning process in zinc crystals the present work is devoted to a study of the growth aspect of the twins.

According to Barrett (1), crystals are said to be twinned if they are composed of portions that are joined together with "a definite mutual orientation." A more general and complete definition was made by Cahn (2):

> "A twin may be defined as a polycrystalline edifice, built up of two or more homogeneous portions of the same crystal species in juxtaposition, and oriented with respect to each other to 'well defined laws'."

The orientation relationship between two neighboring portions of a twin is such that they can be brought into one congruent orientation by a reflection with respect to a lattice plane of low indices, or by

a rot

indic

as (i

(iii)

unfav

loadi

been

shea

whic

mate

great

by Ki

in zi

<1̄01

value

that t

of the

numb

by a

the a

subje

it is

metho

with t

a rotation through either $\frac{\pi}{3}$, $\frac{\pi}{2}$, $\frac{2}{3}\pi$, or π about a lattice row of low indices. Twins, according to their origins, are classified by Cahn (2) as (i) growth twins, (ii) thermal and transformation twins, and (iii) mechanical twins.

Zinc crystals are known to twin readily when they are oriented unfavorably for the basal slip system to be operative under particular loading conditions. The $\{10\bar{1}2\} < 10\bar{1}\bar{1} >$ type twin in zinc, which has been known as the sole active twin system, is associated with a twin shear $\gamma = 0.139$. This low γ value satisfies one of the criteria which govern the selection of the possible modes of twinning in a material that the smaller the shear of a possible twin mode, the greater its chance of being operative (3). According to the investigation by Kiho (4), it is the smallest twin shear of all possible twin systems in zinc. The next smallest twin shear $\gamma = 0.467$ for the $\{10\bar{1}1\}$ $< \bar{1}012 >$ type twin is more than three times larger than the above value.

Another criterion for the choice of a favorable twin system is that the twinning process should involve the least amount of reshuffling of the atoms in the crystal. It is known that only a fraction of the total number of atoms in a zinc crystal can be brought to the twinned positions by a homogeneous shear (5), (6), and (3). A reshuffling of the rest of the atoms is necessary. The reshuffling mechanism is a controversial subject. It is not included in the present work, not for the reason that it is unimportant, but rather because there is yet no known experimental method by which a certain reshuffling mechanism can be verified. Thus, with the crystallography of the twin in zinc crystals known, mechanical

twinning in this material is treated in the usual way as a problem of the nucleation and the growth of the twin.

For the homogeneous nucleation of twins one may use an expression similar to that for the slip process (7) to estimate the critical resolved shear stress (C.R.S.S.) for twinning $= K_t \gamma / 2\pi$, where K_t is the transformed shear modulus on the twin plane in the twinning direction. For the $\{10\bar{1}2\} <10\bar{1}\bar{1}>$ type twins in zinc K_t has been calculated to be 4.08×10^{11} dynes/cm^2. Substituting this value and $\gamma = 0.139$, a C.R.S.S. for twinning $\cong 90$ kg/mm^2 is obtained. The fact that twins are formed in zinc under widely varying resolved shear stresses from about 80 to 4,400 g/mm^2 suggests that either a local stress concentration or some type of dislocation mechanism, or both are necessary for the twinning process.

Cottrell and Bilby (8) proposed a dislocation pole mechanism for the nucleation and growth of twins in the body-centered cubic structure. The essence of the pole mechanism is that a partial twin dislocation rotates about a sessile pole dislocation to form a helix which expands under stress. The formation of a twin requires only one twin dislocation resulted from a dislocation dissociation process. If mechanical twinning in a given crystal is to be described by this mechanism, the following conditions must be satisfied:

(i) The sweeping dislocation must produce the right shear displacement to generate the transformed structure on the sweeping plane.

(ii) The Burgers vector of the pole dislocation must have a component perpendicular to the sweeping plane that is equal to the spacing of these planes.

(iii) The pole dislocation must be anchored strongly enough to prevent it from moving under the stress causing the sweeping dislocation to move.

(iv) The sweeping and pole dislocations, together perhaps with other associated dislocation lines, must be concurrent at a node which acts as an anchor point and around it the sweeping dislocation must be free to move in a sweeping plane which is intersected by the pole.

The formation of the $\{112\}<11\bar{1}>$ type twin in the body-centered cubic structure can be accounted for with the pole mechanism where these conditions are found to be fully satisfied. In the case of the $\{11\bar{1}\}<112>$ type twin in the face-centered cubic structure, however, the second part of the last condition (iv) is not satisfied; consequently only monolayer twins could be formed. This conclusion was regarded as especially satisfactory because at the time the pole mechanism was advanced no one had demonstrated unambiguously that mechanical twins could also be formed in face-centered cubic crystals. In hexagonal close-packed cadmium, Thompson and Millard (9) considered a screw dislocation along the c axis, a "major dislocation", which was intersected at some point by the $\{10\bar{1}2\}$ composition plane of the twin. They proposed that a dissociation of the "major dislocation" would initiate a pole mechanism similar to that proposed by Cottrell and Bilby (8). They (9) contended that all four of the necessary conditions for the pole mechanism were satisfied by the mechanism they introduced. So far there has been no experimental evidence to substantiate Thompson and Millard's theory.

More contributions have been made to the understanding of the twinning process in body-centered cubic crystals in recent years. Sleeswyk and Verbraak (10) studied the incorporation of slip dislocations

at the coherent twin boundary and arrived at a mechanism to account for the twin growth. Sleeswyk (11) observed also the so-called "emissary dislocations" emanating from the incoherent twin tips. According to him, an "emissary dislocation" is a dissociation product of the twin dislocation at the incoherent twin tip accompanying a "complementary twin dislocation". Votava and Sleeswyk (12) showed by a study with transmission electron microscopy of a Mo-35 at. % Re alloy that there were two types of emissary dislocation arrays. Fragmentation of the twin lamellae often resulted due to the incorporation of certain slip dislocations. Ogawa and Maddin (13) also studied the twinning in Mo-Re alloys with transmission electron microscopy and proposed a modified pole mechanism that three-layer twins, also called "emissary sets", could be generated from slip dislocations and grow by means of a "super pole mechanism".

In β-tin crystals Ishii and Kiho studied the incorporation of slip dislocations in mechanical twins (14) and the resistive stress required for the thickening of the twins (15). They considered all the slip dislocations as the pure screw type and arrived at a model similar to that proposed by Thompson and Millard. Fourie et al. (16) examined the nucleation and growth of twins in tin by transmission electron microscopy. They showed consistent evidence to support the assumption that an advancing non-coherent twin interface consists of an array of twin dislocations. The mechanism by which a twin might widen as a result of the production of additional twin dislocations was not disclosed by their observation.

The fact that mechanical twinning does occur in face-centered cubic metals was indisputably established first by Blewitt et al. (17), who found that Cu single crystals of certain orientations twinned under high stresses at 77°K and 4.2°K. Suzuki and Barrett (18) found in tensile tests at low temperatures that mechanical twinning occurred in Ag-Au alloy single crystals of suitable orientation throughout the entire range of alloy composition. In attempting to rationalize these experimental results, Venables (19) arrived at a dislocation mechanism by extending the pole mechanism and allowing the associated dislocation to slip "prismatically" from one plane to the next after each revolution of the twin dislocation. Cohen and Weertman (20) suggested a dislocation dissociation mechanism for twinning in the face-centered cubic metals that twin dislocations are produced by the dissociation of slip dislocations which are in a pile-up state of the Lomer-Cottrell lock and move under the applied stress to form a twin. Venables studied mechanical twinning in single crystals of face-centered cubic Cu alloys by transmission electron microscopy (21) and presented in a subsequent article (22) a calculation of the stress required for twin nucleation in terms of stacking fault energy and an analysis of the dynamics of twin propagation.

Another fundamental concept on twinning besides the dislocation mechanism is the homogeneous twin nucleation suggested by Orowan (23). He introduced a model that a lenticular twin lamella is bounded by twin dislocation loops. According to Orowan's calculation, homogeneous formation of mechanical twins can take place with the aid of a local stress concentration in the absence of any thermal activation. The work of Bell and Cahn (24) shows that twinning in hexagonal close-packed zinc occurred after both the second-order pyramidal and the basal slips had

taken place. They concluded that the twin nucleus was created locally as an entity by a homogeneous shear of the lattice at the site of sufficient stress concentration produced by the pile-up of slip dislocations against a suitable obstacle. Price (25) studied twinning in dislocation-free zinc platelets by deforming the samples inside an electron microscope. He concluded that twins were nucleated at regions where there was a stress concentration in the absence of any dislocations, and that twins grew by the repeated nucleation at the platelet edges and movements of twin dislocations. He also considered some possible dislocation reactions at the twin boundary.

From the above review it is seen that twinning and slip are interdependent in the course of plastic deformation. The degree of mutual influence depends to a marked degree upon the orientation of the crystal and the loading conditions. Certain configuration of the slip dislocations may result in a state of dislocation pile-up. The stress concentration due to the pile-up may in turn enhance the process of twin nucleation as well as twin growth. On the other hand, twins dispersed in the crystal can act as effective barriers against moving slip dislocations. The slip dislocations which move up against the coherent twin boundary will have to either pile up against the latter or be incorporated into the twin.

In the present work an attempt will be made to analyze the growth of the $\{10\bar{1}2\}\langle 10\bar{1}\bar{1}\rangle$ type twins in zinc crystals as a result of the incorporation of slip dislocations at the coherent twin boundary by extending the method advanced by Sleeswyk and Verbraak (10). It is assumed that such a twin bounded by coherent twin boundaries is present

in the crystal, and that appreciable deformation by slip has taken place prior to the twin formation. Geometric and energetic factors will be considered in the analysis.

Zinc has a hexagonal close-packed structure with the lattice parameters $a = 2.6649\ \text{Å}$ and $c = 4.9468\ \text{Å}$ $(c/a = 1.856)$ at room temperature (26). The five independent elastic constants of zinc single crystals (27), and the elastic moduli and Lamé's constants of polycrystalline zinc (28) are listed in Table 1. Since the c axis of the hexagonal lattice is a unique six-fold symmetry axis, the elastic properties of zinc single crystal are axially symmetric about the c axis or transversely isotropic. Most of the available solutions of the stress fields around dislocations, their elastic energies, and the discussions of the interaction between dislocations are based on isotropic elasticity theory, which is oftentimes inadequate even for cubic crystals. For the hexagonal zinc crystal an application of the anisotropic elasticity theory is deemed necessary.

The following is an outline of the scheme used in the present work:

1. Calculate the elastic energies of the dislocations of the various slip systems and the twin system.
2. Calculate the stress field around a twin dislocation and investigate the interaction between twin dislocations.
3. Choose proper coordinate systems for both the matrix and the twin.
4. Derive a matrix equation for expressing a vector in the matrix in terms of the coordinate system chosen for the twin.

5. Derive another matrix equation for expressing the same vector with the coordinate system of the twin after applying to this vector a homogeneous shear corresponding to the twinning action.

6. Find the difference of the two matrix equations thus derived, a matrix equation for the homogeneous twin shear.

7. Apply the equations on various slip vectors of the active slip systems at room temperature to find the corresponding slip vectors in the twin and the associated twinning actions.

8. Examine all the possible equations from energetic and geometric points of view.

9. Find the feasible mechanism or mechanisms for the twin growth by the incorporation of slip dislocations.

10. Prepare zinc single crystals of various orientations and design specific ways of loading to test the validity of the mechanisms.

11. Interpret and discuss the experimental results in the light of the theory thus developed.

S_1

0.8

C_1

16.

*

a

Table 1. Elastic Constants of Zinc Crystal

Elastic compliance constants (10^{-12} cm^2/dyne)						
S_{11}	S_{12}	S_{13}	S_{33}	S_{44}	$S_{66} = 2(S_{11}-S_{12})$	Ref.
0.838	0.053	-0.731	2.838	2.610	1.570	27

Elastic stiffness constants (10^{11} dynes/cm^2)						
C_{11}	C_{12}	C_{13}	C_{33}	C_{44}	$C_{66} = 1/2(C_{11}-C_{12})$	Ref.
16.10	3.35*	5.01	6.10	3.83	6.38	27

Elastic constants (observed) of polycrystalline zinc (10^{11} dynes/cm^2)				
E	G	λ	μ	Ref.
9.22	3.72	6.92	3.72	28

* The correct value of C_{12} from the inversion of S_{ij}'s is 3.35 and not 3.42 as given in the reference.

II. THEORY

1. Application of anisotropic elasticity theory to dislocations in zinc

The anisotropic elasticity theory of dislocations was developed by Burgers (29), Eshelby (30), Leibfreid (31), Eshelby, Read, and Shockley (32), and Seeger and Schöck (33). Eshelby et al. derived the general elastic solution for a straight dislocation of any orientation in an anisotropic crystal. Although anisotropic elasticity theory has been applied to a few crystal structures, only its application to hexagonal crystals will be discussed here.

Foreman (34) calculated the elastic energy of a straight dislocation with a Burgers vector in the close-packed direction. Chou and Eshelby (35) derived an expression for the energy of a circular dislocation loop and calculated the line tension of a dislocation. The width of an extended dislocation (36) and the interaction between parallel dislocations (37) have been investigated by Chou.

1.1. Elastic energies of dislocations

Foreman (34) has shown that the elastic energy per unit length of a straight dislocation line of either edge, mixed, or screw character in an anisotropic crystal is given by

$$E = \frac{Kb^2}{4\pi} \ln \left(\frac{R}{r_o}\right) , \qquad (1\text{-}1)$$

where R is the radius of the dislocation strain field, r_o is the radius of the dislocation core, b is the magnitude of the Burgers vector, and

K is a function of the elastic constants of the crystal and orientation of both the Burgers vector and the dislocation with respect to the crystal axes. Fig. 1 shows the various slip systems and twin system considered. The transformation of the elastic constants obeys the law for the transformation of a fourth-rank tensor. (See Appendix A)

$$C'_{ijkl} = a_{im}\, a_{jn}\, a_{ko}\, a_{lp}\, C_{mnop} \qquad (1\text{-}2)$$

$$S'_{ijkl} = a_{im}\, a_{jn}\, a_{ko}\, a_{lp}\, S_{mnop} \qquad (1\text{-}3)$$

The complete expansion for any stiffness or compliance can be conveniently obtained by using the "table of composite equation" for transforming stiffnesses and compliances (28).

Let it be defined that the z axis of a right-handed Cartesian coordinate system is parallel to the dislocation line under consideration, and the y axis is perpendicular to the slip plane. The direction cosines a_{ij}'s for the coordinate transformation, where $m = \cos\theta$ and $n = \sin\theta$, and the transformed elastic constants are tabulated in Table 2. As an example the coordinate transformation for the $\{10\bar{1}2\}\langle 10\bar{1}\bar{1}\rangle$ type twin considered is illustrated in Fig. 2. The S^*_{ij}'s relate the strain and the stress of the plane strain elastic state around an edge dislocation according to the following equation (30):

$$\begin{pmatrix} \epsilon_{xx} \\ \epsilon_{yy} \\ \epsilon_{xy} \end{pmatrix} = \begin{pmatrix} S^*_{11} & S^*_{12} & S^*_{16} \\ S^*_{12} & S^*_{22} & S^*_{26} \\ S^*_{16} & S^*_{26} & S^*_{66} \end{pmatrix} \begin{pmatrix} \sigma_{xx} \\ \sigma_{yy} \\ \sigma_{xy} \end{pmatrix} \qquad (1\text{-}4)$$

where

$$S^{*}_{ij} = \frac{\begin{vmatrix} S'_{ij} & S'_{i3} & S'_{i4} & S'_{i5} \\ S'_{3j} & S'_{33} & S'_{34} & S'_{35} \\ S'_{4j} & S'_{43} & S'_{44} & S'_{45} \\ S'_{5j} & S'_{53} & S'_{54} & S'_{55} \end{vmatrix}}{\begin{vmatrix} S'_{33} & S'_{34} & S'_{35} \\ S'_{43} & S'_{44} & S'_{45} \\ S'_{53} & S'_{54} & S'_{55} \end{vmatrix}} \quad (i, j=1, 2, \text{or } 6) \qquad (1\text{-}5)$$

1.1.1. Calculation of K from analytic solution

In general it is necessary to find the six complex parameters which are the roots of a sextic equation in order to obtain K for a straight dislocation in an anisotropic crystal (32). However, there are special cases for which analytic solutions exist. For example, in the case of hexagonal crystals if the dislocation line lies parallel to a symmetry axis and perpendicular to a symmetry plane, then the solution K for an edge dislocation is given by (34)

$$K = (\bar{C}_{11} + C'_{12})\left[\frac{C'_{66}(\bar{C}_{11} - C'_{12})}{C'_{22}(\bar{C}_{11} + C'_{12} + 2C'_{66})}\right]^{1/2}, \qquad (1\text{-}6)$$

where $\bar{C}_{11} = (C'_{11}C'_{22})^{1/2}$. For a screw dislocation

$$K = (C'_{44}C'_{55} - C'^{2}_{45})^{1/2} . \qquad (1\text{-}7)$$

For the edge dislocations of the slip systems, (i) $\{0001\}\langle 11\bar{2}0\rangle$, (ii) $\{1\bar{1}00\}\langle 11\bar{2}0\rangle$, and (v) $\{hk.0\}\langle 0001\rangle$, the

condit

systen

same

(30).

syster

<11$\bar{2}$0

dynes

K = 3.

unique

invari

1.1.2

menti

Nume

secon

dicula

dimer

direct

conditions stated above are satisfied. Therefore, K values for these systems are obtained from Eq. (1-6) and are tabulated in Table 2. The same values may be obtained using the equations developed by Eshelby (30). Chou (37) reported the same K values for these systems.

For screw dislocations Eq. (1-7) can be applied only to the slip systems, (i) $\{0001\}\langle 11\bar{2}0\rangle$, (ii) $\{1\bar{1}00\}\langle 11\bar{2}0\rangle$, (iii) $\{1\bar{1}01\}\langle 11\bar{2}0\rangle$, and (v) $\{hk.0\}\langle 0001\rangle$. A value of $K = 4.94 \times 10^{11}$ dynes/cm^2 is obtained for the systems (i), (ii), and (iii), and $K = 3.83 \times 10^{11}$ dynes/cm^2 for the system (v). Since there is no unique slip plane associated with a screw dislocation, K is an invariant for a rotation of the axes about the dislocation line (z axis).

1.1.2. Calculation of K from numerical solution

For the systems that do not satisfy the orientation conditions mentioned in Sec. 1.1.1. the value K can only be solved numerically. Numerical solutions are found for the edge dislocation where only the second condition is satisfied, that is, the dislocation line is perpendicular to a symmetry plane.

Under such a condition the problem is reduced to a two dimensional problem. The results obtained by Eshelby (30) can be directly applied. The expression for K in this case is

$$K = \frac{\begin{vmatrix} \lambda_{1r} & \lambda_{2r} & -(\lambda_{1i} - \lambda_{2i}) \\ \lambda_{1i} & \lambda_{2i} & (\lambda_{1r} - \lambda_{2r}) \\ D_{1r} & D_{2r} & (D_{1i} - D_{2i}) \end{vmatrix}}{\begin{vmatrix} \lambda_{1r} & \lambda_{2r} & -(\lambda_{1i} - \lambda_{2i}) \\ C_{1i} & C_{2i} & (C_{1r} - C_{2r}) \\ D_{1r} & D_{2r} & (D_{1i} - D_{2i}) \end{vmatrix}} , \tag{1-8}$$

where the subscripts r, i denote the real and imaginary parts of a complex quantity respectively. The complex constants λ_1 and λ_2 relate the two complex variables z_n, where $n = 1, 2,$ with two real variables x, y by

$$z_n = x + i\lambda_n y \tag{1-9}$$

where λ_n is given implicitly in terms of the elastic constants by the following relations:

$$\lambda_n = \frac{1 - \gamma_n - i\delta_n}{1 + \gamma_n + i\delta_n} \tag{1-10}$$

$$\gamma_n = \frac{a_n - 1}{a_n + 1 + 2(a_n - \frac{1}{4} k_n^2)^{1/2}} \tag{1-11}$$

$$\delta_n = \frac{-k_n}{a_n + 1 + 2(a_n - \frac{1}{4} k_n^2)^{1/2}} , \tag{1-12}$$

where

$$a_1 + a_2 + k_1 k_2 = \frac{(2S_{12}^* + S_{66}^*)}{S_{22}^*} \tag{1-13}$$

$$\alpha_1 \alpha_2 = \frac{S_{11}^*}{S_{22}^*} \tag{1-14}$$

$$k_1 + k_2 = - \frac{2S_{26}^*}{S_{22}^*} \tag{1-15}$$

$$k_1 \alpha_2 + k_2 \alpha_1 = - \frac{2S_{16}^*}{S_{22}^*} \tag{1-16}$$

where $(\alpha_n - \frac{1}{4} k_n^2)$ and α_n are real and positive; k_n, γ_n, and δ_n are real. C_n and D_n are given by

$$C_n = S_{11}^* \lambda_n^2 - S_{12}^* + i\lambda_n S_{16}^* \tag{1-17}$$

$$D_n = \frac{1}{\lambda_n} (S_{12}^* \lambda_n^2 - S_{22}^* + i\lambda_n S_{26}^*) \quad . \tag{1-18}$$

The orientation of the edge dislocations of the slip system (iv) $\{11\bar{2}2\}<11\bar{2}\bar{3}>$ and the twin systems (x) $\{10\bar{1}2\}<10\bar{1}\bar{1}>$ is such that the dislocation lines are perpendicular to a symmetry plane. But they are not parallel to a symmetry axis, hence $S'_{16} \neq 0$, $S'_{26} \neq 0$ and $S_{16}^* \neq 0$, $S_{26}^* \neq 0$.

The procedure of a numerical calculation is explained for the twin system. First S_{ij}^*'s are calculated from the transformed elastic constants S'_{ij}'s with an aid of Schweins expansion (30). Then on substituting S_{ij}^* into the Eqs. (1-13), (1-14), (1-15), and (1-16) four simultaneous algebraic equations are obtained. These can be reduced to an equation of sixth degree in α_n. The real and positive roots are found to be $\alpha_1 = 3.18$, $\alpha_2 = 0.35$; and correspondingly $k_1 = 0.84$, $k_2 = 0.37$. Substituting these roots into Eqs. (1-12), (1-11), (1-10),

(1-17), and (1-18) successively, one obtains

$$\delta_1 = -0.11 \qquad \delta_2 = -0.15$$
$$\gamma_1 = 0.29 \qquad \gamma_2 = -0.26$$
$$\lambda_1 = 0.60 + 0.13i \qquad \lambda_2 = 1.60 + 0.53i$$
$$C_1 = 0.72 - 0.27i \qquad C_2 = 3.19 + 0.70i$$
$$D_1 = -1.77 - 0.30i \qquad D_2 = -0.96 - 0.56i$$

where C_n and D_n are in units of 10^{-12} cm^2/dyne. From Eq. (1-8) one finds $K = 4.08 \times 10^{11}$ dynes/cm^2 for the twin system. Similarly $K = 3.90 \times 10^{11}$ dynes/cm^2 is found for the $\{11\bar{2}2\}<11\bar{2}\bar{3}>$ slip system.

For the slip systems (iii) $\{1\bar{1}01\}$ $<11\bar{2}0>$, (vii) $\{11\bar{2}2\}$ $<20\bar{2}\bar{3}>$, (ix) $\{1\bar{1}00\}$ $<11\bar{2}\bar{3}>$, and (xi) $\{10\bar{1}1\}$ $<11\bar{2}\bar{3}>$ neither one of the orientation conditions is satisfied by such edge dislocation lines. Numerical calculation for these four systems becomes more complicated involving three complex variables with six complex parameters. K values for the three slip systems (iii), (vii), and (ix) are calculated by assuming that these dislocation lines were perpendicular to the corresponding symmetry planes of the crystal as a first approximation. The actual angles that these dislocation lines deviate from the corresponding normals to the symmetry planes are respectively 25.1°, 15.3°, and 28.3°. It may be noted that this approximation is probably poor for the slip systems (iii) and (ix) but may be close for the slip system (vii).

1.1.3. Elastic energy of edge dislocations

Certain properties of edge dislocation in an anisotropic crystal can be calculated quantitatively once the values of K for the different

slip systems are known. The elastic energy of an edge dislocation is obtained from Eq. (1-1). The numerical value of E depends upon the choice of R and r_o. Except for a factor of $\ln (R/r_o)$ the values of E in ergs per cm of the edge dislocation line are listed in column (10) of Table 3. These values can be considered as the relative energies of the various edge dislocations and can be compared with one another directly. In the last five rows of Table 3 data pertaining to certain partial dislocations are listed.

Eshelby (30) defined a quantity $\zeta = 1/2\ K\ S'_{66}\ d$ as a measure of the width of a dislocation. He also suggested that ζ/b would serve as a measure of the "ease of gliding." These quantities are also calculated and listed in Table 3.

1.2. Interaction of two parallel twin dislocations

Chou (37) derived the equations for the stress field of an edge dislocation and a screw dislocation with $\vec{b} = \frac{1}{3}\ [11\bar{2}0]$ and an edge dislocation with $\vec{b} = [0001]$. As mentioned before, analytic solutions are available for these dislocations. He also analyzed the forces between two parallel dislocations and stress fields of various types of infinite dislocation walls.

In this section the stress field of a twin dislocation in the edge orientation will be calculated and the results will be applied to finding the interaction forces between two parallel twin dislocations.

1.2.1. Stress field of a twin dislocation

As discussed in the previous section, the solution by Eshebly (30)

directly applies to an edge type twin dislocation. Calculated K for the twin system $\{10\bar{1}2\}<10\bar{1}\bar{1}>$ is $K_t = 4.08 \times 10^{11}$ dynes/cm^2 and the magnitude of Burgers vector is $b_t = 0.088\ a = 2.35 \times 10^{-9}$ cm.

The expressions for the stress components are

$$\sigma_{xx} = - \sum_{n=1,2} \lambda_n^2 f_n''(z_n) + c.c. \qquad (1-19)$$

$$\sigma_{yy} = \sum_{n=1,2} f_n''(z_n) + c.c. \qquad (1-20)$$

$$\sigma_{xy} = -i \sum_{n=1,2} \lambda_n f_n''(z_n) + c.c. \qquad (1-21)^*$$

where c.c. represents the complex conjugate of the quantity preceding it and $f_n(z_n)$ is a component of the stress function. For an edge dislocation

$$f_n'(z_n) = \frac{1}{2} A_n \ln z_n \ , \qquad (1-22)$$

where A_n is a complex constant. In order for the total force and the couple on any Burgers circuit to vanish it is necessary that

$$A_{2i} = - A_{1i} \qquad (1-23)$$

$$\lambda_{1r} A_{1r} + \lambda_{2r} A_{2r} - (\lambda_{1i} - \lambda_{2i}) A_{1i} = 0 \ . \qquad (1-24)$$

---

* Eshelby et al.(32) made some corrections of the earlier paper (30). The author finds some misprints in the reference (30) namely that Eq. (1-21)* should have λ_n following the summation sign and the sign of the last term in Eq. (1-26)* should be + instead of - .

If the Burgers vector is $(b_x, 0)$, it follows

$$C_{1i} A_{1r} + C_{2i} A_{2r} + (C_{1r} - C_{2r}) A_{1i} = \frac{b_x}{2\pi} \qquad (1-25)$$

$$D_{1r} A_{1r} + D_{2r} A_{2r} + (D_{1i} - D_{2i}) A_{1i} = 0 \ . \qquad (1-26)^*$$

Again the subscripts r, i denote the real and imaginary parts of a quantity respectively.

Substituting the values of λ_n, C_n, and D_n from Sec. 1.1.2. into Eq!s. (1-24), (1-25), and (1-26), one obtains

$$A_1 = - F (1.25 + 3.53i) \qquad (1-27)$$

$$A_2 = F (1.35 + 3.53i) \ , \qquad (1-28)$$

where $F = b_t / 2\pi \times 10^{11}$ dynes/cm. From Eq. (1-22)

$$f_n'' (z_n) = \frac{1}{2} A_n \frac{1}{z_n} \ . \qquad (1-29)$$

Finally, the expressions for the stress components are obtained by substituting Eq's. (1-27), (1-28), and (1-29) into Eq's. (1-19), (1-20), and (1-21) and rearranging

$$\sigma_{xx} = \frac{K_t b_t}{2\pi} \left[\frac{0.03x - 0.21y}{(x - 0.13y)^2 + 0.36y^2} - \frac{0.72x - 4.44y}{(x - 0.53y)^2 + 2.56y^2} \right] \qquad (1-30)$$

$$\sigma_{yy} = \frac{K_t b_t}{2\pi} \left[\frac{0.31x + 0.48y}{(x - 0.13y)^2 + 0.36y^2} - \frac{0.33x - 1.21y}{(x - 0.53y)^2 + 2.56y^2} \right] \qquad (1-31)$$

$$\sigma_{xy} = \frac{K_t b_t}{2\pi} \left[\frac{0.56x - 0.12y}{(x - 0.13y)^2 + 0.36y^2} - \frac{1.56x - 0.94y}{(x - 0.53y)^2 + 2.56y^2} \right] \qquad (1-32)$$

1.2.2. Interaction between two parallel twin dislocations

The force of one dislocation acting on another can be defined as the gradient of U_I, the interaction energy between them. Following Cottrell (38) the ith component of the force F exerted on one dislocation by the other is

$$F_i = -\frac{\partial U_I}{\partial x_i} \quad . \tag{1-33}$$

The signs of Eq's. (1-30), (1-31), (1-32), and (1-33) have been chosen to be consistent with Frank's convention (39). The components of the force F per unit length exerted on a twin dislocation at (x, y) by another at the origin are (38)

$$F_x = \sigma_{xy} b_t \tag{1-34}$$

$$F_y = \sigma_{xx} b_t \quad . \tag{1-35}$$

If the twin dislocation at (x, y) lies on the adjacent plane, i.e. $y = d$ where $d = 0.633\ a$ is the spacing between neighboring twin planes, then

$$F_x(x, d) = \frac{K_t b_t^2}{2\pi} \left[\frac{0.56x - 0.12d}{(x - 0.13d)^2 + 0.36d^2} - \frac{1.56x - 0.94d}{(x - 0.53d)^2 + 2.56d^2} \right] \tag{1-36}$$

$$F_y(x, d) = \frac{K_t b_t^2}{2\pi} \left[\frac{0.03x - 0.21d}{(x - 0.13d)^2 + 0.36d^2} - \frac{0.72x - 4.44d}{(x - 0.53d)^2 + 2.56d^2} \right] \tag{1-37}$$

These results are plotted in Fig. 3 and Fig. 4. Unlike the isotropic elasticity theory of dislocation F_x becomes noncentrosymmetrical in this case.

1.3. Application

1.3.1. Dislocation reactions

Frank and Nicholas (40) discussed the relative stability of perfect and imperfect dislocations in hexagonal close-packed crystals using the simplified criterion that the line energy of a dislocation is proportional to the square of the absolute value of its Burgers vector. This method would not yield a definite solution of the feasibility of a dislocation dissociation process when the Burgers vectors of the three dislocations involved are the three sides of a right triangle and the Burgers vector of the dissociating dislocation is the hypotenuse. The application of the anisotropic elastic energies of the various components will yield a definite answer to this problem.

Following Eshelby (30), if $D(\vec{b})$ represents a dislocation with a Burgers vector $\vec{b}$, a dislocation dissociation (or association) process may be written as

$$D(\vec{b}_1) + D(\vec{b}_2) \rightleftharpoons D(\vec{b}_3) \qquad (1\text{-}38)$$

where $\vec{b}_1 + \vec{b}_2 = \vec{b}_3$. According to Eq. (1-1) the energy of dissociation may be written as

$$\Delta E = \frac{1}{4\pi} (K_1 b_1^2 + K_2 b_2^2 - K_3 b_3^2) \ln \left(\frac{R}{r_o}\right) . \qquad (1\text{-}39)$$

The reaction will take place in the direction of dissociation or association according to whether ΔE is negative or positive.

Thus the decrease in elastic energy associated with the dissociations of the total dislocations of the basal and the second-order pyramidal slips into extended dislocations are

$$\Delta E = -1.03 \ln (R/r_o) \times 10^{-5} \text{ ergs/cm}$$

for

$$\frac{1}{3}[11\bar{2}0] \longrightarrow \frac{1}{3}[10\bar{1}0] + \frac{1}{3}[01\bar{1}0]$$

or (1-40)

$$-\vec{a}_3 \longrightarrow -\vec{p}_3 + \vec{p}_2 ,$$

and

$$\Delta E = -4.21 \ln (R/r_o) \times 10^{-5} \text{ ergs/cm}$$

for

$$\frac{1}{3}[11\bar{2}\bar{3}] \longrightarrow \frac{1}{6}[20\bar{2}\bar{3}] + \frac{1}{6}[02\bar{2}\bar{3}]$$

or (1-41)

$$-(\vec{c} + \vec{a}_3) \longrightarrow -(\vec{p}_3 + \frac{1}{2}\vec{c}) + (\vec{p}_2 - \frac{1}{2}\vec{c}) ,$$

where the vectors $<\vec{a}>$ and $\vec{c}$ are the Burgers vectors of the total dislocations and $<\vec{p}>$ and $<\vec{p} + 1/2\,\vec{c}>$ are those of the partial dislocations. Fig. 5 gives a representation of these Burgers vectors, which is similar to that given by Price (41).

The following two dislocation reactions, which are energetically reversible from the isotropic elasticity point of view, become unidirectional toward dissociation from the anisotropic elasticity point of view:

$$\Delta E = -0.25 \ln (R/r_o) \times 10^{-5} \text{ ergs/cm}$$

for

$$\frac{1}{3}[11\bar{2}\bar{3}] \longrightarrow \frac{1}{3}[11\bar{2}0] + [000\bar{1}]$$

or (1-42)

$$-(\vec{c} + \vec{a}_3) \longrightarrow -\vec{a}_3 - \vec{c} ,$$

and

$$\Delta E = -0.15 \ln (R/r_o) \times 10^{-5} \text{ ergs/cm}$$

for

$$\frac{1}{6}[\,20\bar{2}\bar{3}] \longrightarrow \frac{1}{3}[\,10\bar{1}0] + \frac{1}{2}[\,000\bar{1}]$$

or (1-43)

$$-(\vec{p}_3 + \frac{1}{2}\vec{c}) \longrightarrow -\vec{p}_3 - \frac{1}{2}\vec{c} \quad .$$

Perhaps it is of interest to note that, judging from Eshelby's criterion for the ease of gliding ζ/b as listed in Table 3 for the various slip processes, the order in increasing difficulty is; basal slip, second-order pyramidal slip, first-order pyramidal slip, prismatic slip, prismatic slip with $\vec{b} = 1/6 < 11\bar{2}\bar{3} >$, and normal slip. Such an order seems to agree with existing observations.

1.3.2. Incoherent twin boundaries

The interaction forces between two parallel twin dislocations of edge orientation have been calculated in Sec. 1.2.2. and plotted in Fig. 3 and Fig. 4. The F_x component of the interaction force is of significance since it acts in the direction of the twin shear. As illustrated in Fig. 3, $F_x = 0$ when $x/d = 1.31$, -0.07, or -0.56. These are the neutral positions of the twin dislocation in the absence of applied stresses.

There exist two maxima of the interaction force per unit length of dislocation line:

$$F_1 = 0.204 \frac{K_t b_t^2}{2\pi d} \qquad \text{at} \quad \frac{x_1}{d} = -2.45 \tag{1-44}$$

$$F_2 = 0.360 \frac{K_t b_t^2}{2\pi d} \qquad \text{at} \quad \frac{x_1}{d} = 0.528 \quad . \tag{1-45}$$

The critical shear stress τ_1 to overcome the first maximum repulsive force F_1 can be found by equating the driving force $F_d = \tau_1 b_t$ and F_1:

$$\tau_1 \cong 0.20 \frac{K_t}{2\pi} \gamma \cong 19 \text{ kg/mm}^2 , \qquad (1-46)$$

where $\gamma = b_t/d = 0.139$ is the shear strain associated with the $\{10\bar{1}2\}$ $<10\bar{1}\bar{1}>$ type twin in zinc. Similarly for the second maximum the critical shear stress is

$$\tau_2 \cong 0.36 \frac{K_t}{2\pi} \cong 33 \text{ kg/mm}^2 \qquad (1-47)$$

The shape of the advancing twin interfaces depends mainly upon the applied shear stress and the interaction between the twin dislocations. It can be discussed with the aid of the schematic diagrams in Fig. 6. Assume that n twin dislocations with equal Burgers vector are situated on successive atomic planes and form a coherent group. If the leading dislocation is halted by an obstacle the force acting on the immediately following dislocation will be

$$F_d = (n - 1) \tau_a b_t \qquad (1-48)$$

where τ_a is the applied resolved shear stress. If F_d is smaller than F_1 the configuration shown in Fig. 6(a) is stable. θ_1 must be smaller than arctan (d/x_1) or 22°. If F_d is greater than F_1 but smaller than F_2 the configuration shown in Fig. 6(b) is a possible one. In this case arctan $(1/0.07) < \theta_2 <$ arctan $(-d/x_2)$ or $86^\circ < \theta_2 < 118^\circ$. If the mth dislocation is halted by an obstacle and the force acting on the $(m + 1)$th dislocation is momentarily greater than F_2, the configuration shown in Fig. 6(c) may result.

1.3.3. Coherent twin boundary energy

In the absence of an effective obstacle the advancement of the twin interfaces will be limited by the increase in energy associated with the increase in area of the coherent twin boundaries. Thus the angle θ provides an estimate of the coherent twin boundary energy γ_t. If the position of the leading twin dislocation is varied by δx from its equilibrium position the area of the coherent twin boundaries will be increased by $2\delta x$ per unit length of the twin dislocation line. Hence

$$2\gamma_t \delta x = F_d \delta x \qquad (1-49)$$

or $\gamma_t = F_d/2$. F_d can be evaluated from observed θ and Fig. 3.

2. Transformation of indices

2.1. Derivation of transformation matrices

Fig. 7 shows the four coordinate systems chosen. $\vec{a}_1$, $\vec{a}_2$, and $\vec{c}$ are the base vectors which define the hexagonal lattice of the matrix. $\vec{n}_1$, $\vec{n}_2$, and $\vec{n}_3$ are three vectors chosen in such a way that a rotation of π about $\vec{n}_1$ will bring $\vec{a}_1$, $\vec{a}_2$, and $\vec{c}$ respectively to $\vec{a}_1'$, $\vec{a}_2'$, and $\vec{c}'$, the corresponding base vectors in the twin, and $\vec{n}_1$, $\vec{n}_2$, and $\vec{n}_3$ to $\vec{n}_1'$, $\vec{n}_2'$, and $\vec{n}_3'$ respectively.

Thus any vector can be described equally well by using one of the four coordinate systems. For instance,

$$\vec{X} = X_1\vec{a}_1 + X_2\vec{a}_2 + X_3\vec{c}$$

$$\vec{N} = N_1\vec{n}_1 + N_2\vec{n}_2 + N_3\vec{n}_3$$

$$\vec{N}' = N_1'\vec{n}_1' + N_2'\vec{n}_2' + N_3'\vec{n}_3'$$

$$\vec{X}' = X_1'\vec{a}_1' + X_2'\vec{a}_2' + X_3'\vec{c}'$$

or

$$\begin{aligned} \underline{X} &= (X_1\ X_2\ X_3) \\ \underline{N} &= (N_1\ N_2\ N_3) \\ \underline{N}' &= (N_1'\ N_2'\ N_3') \\ \underline{X}' &= (X_1'\ X_2'\ X_3') \end{aligned} \tag{2-1}$$

In order that $\vec{X}$, $\vec{N}$, $\vec{N}'$, and $\vec{X}'$ are to represent the same vector the vector components in the four coordinate systems must be related in a certain way. The relationships may best be described by using matrix algebra.

Since

$$\begin{aligned} \vec{n}_1 &= \vec{a}_1 - \vec{a}_2 - \vec{c} \\ \vec{n}_2 &= -\vec{a}_1 + \vec{a}_2 - \vec{c} \\ \vec{n}_3 &= \vec{a}_1 + \vec{a}_2 \end{aligned}$$

or

$$\begin{pmatrix} n_1 \\ n_2 \\ n_3 \end{pmatrix} = \begin{pmatrix} 1 & -1 & -1 \\ -1 & 1 & -1 \\ 1 & 1 & 0 \end{pmatrix} \begin{pmatrix} a_1 \\ a_2 \\ c \end{pmatrix}. \tag{2-2}$$

Then the components of $\vec{X}$ and $\vec{N}$ are related by (see for instance reference 42)

$$(X_1\ X_2\ X_3) = (N_1\ N_2\ N_3) \begin{pmatrix} 1 & -1 & -1 \\ -1 & 1 & -1 \\ 1 & 1 & 0 \end{pmatrix}$$

or

$$\underline{X} = \underline{N}\,\underline{A} \tag{2-3}$$

where

$$\underline{A} = \begin{pmatrix} 1 & -1 & -1 \\ -1 & 1 & -1 \\ 1 & 1 & 0 \end{pmatrix} \tag{2-4}$$

which means upon multiplying,

$$X_1 = (N_1 - N_2 + N_3)$$

$$X_2 = (-N_1 + N_2 + N_3)$$

$$X_3 = (-N_1 - N_2) \quad .$$

It follows from Eq. (2-3) that

$$\underline{N} = \underline{X}\,\underline{A}^{-1} \tag{2-5}$$

where

$$\underline{A}^{-1} = \frac{1}{4} \begin{pmatrix} 1 & -1 & 2 \\ -1 & 1 & 2 \\ -2 & -2 & 0 \end{pmatrix} \tag{2-6}$$

is the inverse of the matrix $\underline{A}$.

Similarly,

$$\vec{n}_1' = \vec{n}_1$$

$$\vec{n}_2' = e\vec{n}_1 - \vec{n}_2$$

$$\vec{n}_3' = \quad\quad - \vec{n}_3 \quad , \tag{2-7}$$

where e is a numerical factor such that $e\vec{n}_1$ is the projection of $\vec{n}_2'$ in $\vec{n}_1$ (also $\vec{n}_1'$). For zinc $e = 0.069$ and $|e\vec{n}_1| = 0.176$ a,

a is the spacing of atoms in the close-packed plane. Let

$$\underline{R} = \begin{pmatrix} 1 & 0 & 0 \\ e & -1 & 0 \\ 0 & 0 & -1 \end{pmatrix} \tag{2-8}$$

then

$$\underline{N} = \underline{N}' \underline{R} \tag{2-9}$$

and

$$\underline{N}' = \underline{N} \underline{R}^{-1} = \underline{N} \underline{R} \ . \tag{2-10}$$

It is necessary that $\underline{R} = \underline{R}^{-1}$ since $\underline{N} \underline{R} \underline{R} = \underline{N}$ is equivalent to a rotation of 2π about n_1, which must leave $\underline{N}$ unchanged. It follows, therefore, that $\underline{R} \underline{R} = \underline{I}$ and hence $\underline{R} = \underline{R}^{-1}$.

The transformation from N' to X' can be written as

$$\underline{X}' = \underline{N}' \underline{A} \ . \tag{2-11}$$

Thus

$$\underline{X}' = \underline{N}' \underline{A} = \underline{N} \underline{R} \underline{A} = \underline{X} \underline{A}^{-1} \underline{R} \underline{A}$$

or

$$\underline{X}' = \underline{X} \underline{T} \tag{2-12}$$

where

$$\underline{T} = \underline{A}^{-1} \underline{R} \underline{A} = \frac{1}{4} \begin{pmatrix} -2-e & -2+e & -2+e \\ -2+e & -2-e & 2-e \\ -4-2e & 4+2e & 2e \end{pmatrix} . \tag{2-13}$$

A vector $\vec{X}$ originally expressed in the $\vec{a}_1$, $\vec{a}_2$, and $\vec{c}$ coordinate system can be expressed in terms of the base vectors $\vec{a}_1'$, $\vec{a}_2'$, and $\vec{c}'$ as $\vec{X}'$ using the matrix equation (2-12).

The twinning action can be conveniently introduced as a homogeneous shear of the vector $\vec{N}$. Let

$$\vec{E} = E_1\vec{n}_1 + E_2\vec{n}_2 + E_3\vec{n}_3 \tag{2-14}$$

to be the vector which is different from $\vec{N}$ but represents the vector $\vec{N}$ after the twin shear, then

$$\begin{aligned} E_1 &= (N_1 - eN_2) \\ E_2 &= N_2 \\ E_3 &= N_3 \ . \end{aligned} \tag{2-15}$$

Let

$$S^T = \begin{pmatrix} 1 & -e & 0 \\ 0 & 1 & 0 \\ 0 & 0 & 1 \end{pmatrix} \tag{2-16}$$

then

$$\underline{E} = \underline{S}^T \underline{N} \tag{2-17}$$

or

$$\underline{E} = \underline{N}\,\underline{S} \ , \tag{2-18}$$

where

$$\underline{S} = \begin{pmatrix} 1 & 0 & 0 \\ -e & 1 & 0 \\ 0 & 0 & 1 \end{pmatrix} \ , \tag{2-19}$$

which is the transpose of $\underline{S}^T$.

Thus a vector $\vec{X}$ will be transformed into $\vec{X}^*$ after the twin shear, if $\vec{X}^*$ is to be expressed in the coordinate system of $\vec{a}_1'$, $\vec{a}_2'$, and $\vec{c}'$ as $\underline{X}^* = (X_1^* \ X_2^* \ X_3^*)$. Therefore,

$$\underline{X}^* = \underline{X}\,\underline{A}^{-1}\underline{S}\,\underline{R}\,\underline{A}$$

or

$$\underline{X}^* = \underline{X}\,\underline{T}^* \tag{2-20}$$

where

$$\underline{T}^* = \underline{A}^{-1}\underline{S}\,\underline{R}\,\underline{A} = -\frac{1}{2}\begin{pmatrix} 1 & 1 & 1 \\ 1 & 1 & -1 \\ 2 & -2 & 0 \end{pmatrix} . \tag{2-21}$$

After a homogeneous shear corresponding to the twinning action is applied to the vector $\vec{X}$, it is transformed into another vector $\vec{X}^*$ according to the matrix equation (2-20).

The difference between $\vec{X}^*$ and $\vec{X}'$ represents the homogeneous shear applied to the vector $\vec{X}$. Thus

$$\underline{X}^* - \underline{X}' = \underline{X}\,\underline{T}^* - \underline{X}\,\underline{T} = \underline{X}\,(\underline{T}^* - \underline{T}) = \underline{X}\,\underline{B} \tag{2-22}$$

where

$$\underline{B} = \underline{T}^* - \underline{T} = \frac{1}{4}\,e\begin{pmatrix} 1 & -1 & -1 \\ -1 & 1 & 1 \\ 2 & -2 & -2 \end{pmatrix} . \tag{2-23}$$

Multiplying the original vector $\vec{X}$ by the matrix $\underline{B}$ according to the matrix equation (2-22), one obtains the homogeneous shear applied to the vector.

2.2. Transformation of indices of Burgers vectors

The slip systems observed in zinc crystals at room temperature are the basal slip and the second-order pyramidal slip. The slip vectors are respectively $\langle \vec{a} \rangle$ and $\langle \vec{c} + \vec{a} \rangle$. Multiplying these vectors by $\underline{T}^*$ and by $\underline{B}$, one obtains the transformed vectors after

the twin shear and the corresponding twin actions respectively. The results are listed in Table 4. The subscripts m and t indicate the matrix and the twin respectively, and

$$\vec{b}_t = \frac{1}{4} e (\vec{a}'_1 - \vec{a}'_2 - \vec{c}') = \frac{1}{2} e \vec{n}_1 \qquad (2\text{-}24)$$

is a vector in the twinning direction $\vec{n}_1$ and may be considered as a unit twin vector or the Burgers vector of a twin dislocation. The magnitude of the Burgers vector of the twin dislocation is 0.088 a.

2.3. Transformation of indices of slip planes

The vectors $\frac{1}{2}[\bar{1}11]_m$, $\frac{1}{2}[\bar{1}\bar{1}1]_m$, and $[\bar{1}10]_m$ will be transformed into $\vec{a}'_1$, $\vec{a}'_2$, and $\vec{c}'$ respectively after the twin shear is applied to them. Thus a plane (hkl) in the matrix is transformed into (HKL) in the twin according to the following equations:

$$H = -\frac{1}{2}h - \frac{1}{2}k - \frac{1}{2}l$$

$$K = -\frac{1}{2}h - \frac{1}{2}k + \frac{1}{2}l$$

$$L = -h + k$$

or in matrix notation

$$(HKL) = (hkl)\,\underline{M} \qquad (2\text{-}25)$$

where

$$\underline{M} = -\frac{1}{2}\begin{pmatrix} 1 & 1 & 2 \\ 1 & 1 & -2 \\ 1 & -1 & 0 \end{pmatrix} \qquad (2\text{-}26)$$

is the transpose of $\underline{T}^*$.

On multiplying the Miller indices of a slip plane in the matrix with $\underline{M}$, one obtains the Miller indices of the corresponding plane in the twin. The transformations of the slip planes are listed in Table 5.

3. Incorporation of slip dislocations at a coherent twin boundary

A dislocation line is defined in general by its Burgers vector, its orientation, and its slip plane. Even a screw dislocation may not glide on an arbitrary crystallographic plane because of crystal anisotropy. Therefore, the slip plane as well as the Burgers vector of a dislocation will have to be considered for an incorporation process. A dislocation approaching the coherent twin boundary would probably be a portion of an expanding loop. The orientation of the portion of the dislocation incorporated into the twin should be that of a dislocation line which is tangent to the dislocation loop and lies in the coherent twin boundary, or parallel to the line of intersection of the slip plane and the coherent twin boundary. Unless this portion of the dislocation line happens to be in pure screw orientation, it can not glide on crystallographic planes in the twin other than those listed in Table 5.

It is also true that the Burgers vector of a mobile dislocation is in general a low index vector which is in a densely packed direction, and that the slip plane is a low index plane which has a high atomic density. On examining Tables 4 and 5, it is concluded that the incorporation of the dislocations described by (6), (7), (8), and (9), are not likely to take place since high index directions and planes are involved. The remaining five types of dislocation incorporation processes are of particular interest and will be discussed one by one.

3.1. Incorporation process (1)

The incorporation process described in (1) means that for the $(1\bar{1}2)[1\bar{1}\bar{1}]$ twin the basal slip vector $[110]_m$ in the matrix is not

affected by the twinning action since it is parallel to the twin plane $(1\bar{1}2)$. Furthermore, it is also parallel to the line of intersection, $[110]_m$ or $[\bar{1}\bar{1}0]_t$, of the basal plane in the matrix, the basal plane in the twin, and the coherent twin boundary $(1\bar{1}2)_{m,t}$. Thus a dislocation with the $[110]_m$ Burgers vector will be in screw orientation when it meets the coherent twin boundary. It can be incorporated into the twin and glide in the basal plane of the twin provided that there is a suitable stress field. The line energy of the dislocation before and after the incorporation process remains the same and hence this process as sketched in Fig. 8 is energetically feasible. This process, however, will not cause the twin either to grow or to shrink since there is no change in either the direction or the magnitude of the Burgers vector. Each dislocation of this type on passing through the matrix and the twin will form a step on the crystal surface (110) along the slip traces. A series of such dislocations will form a macroscopic step.

3.2. Incorporation process (2) and (3)

The dislocation reactions (2), (3), (4), and (5) are important to the growth of twins. The reaction (2) means that the basal slip vector $[100]_m$ in the matrix is sheared into $1/2[\bar{1}\bar{1}1]_t$ upon being incorporated into the twin. The quantity of the twin shear applied to this vector is b_t as defined by Eq. (2-22). The vector $1/2[\bar{1}\bar{1}1]_t$ is common to both the second-order pyramidal plane $(11\bar{2})_t$ and the first-order prism plane $(\bar{1}10)_t$. However, because of the fact that the vector $[100]_m$ is oblique to the coherent twin boundary, the portion of the dislocation incorporated is mixed in nature as discussed previously, and hence it can probably glide only on $(\bar{1}10)_t$ at least at the beginning of the incorporation process.

This process encounters two difficulties which may not be unsurmountable. The first difficulty is that the first-order prism plane is not a favorable slip plane at room temperature, nor $[\bar{1}\bar{1}\bar{1}]_t$ a favorable slip direction (see Table 3). The second difficulty is that the vector $1/2[\bar{1}\bar{1}\bar{1}]_t$ must be associated with a stacking fault on $(\bar{1}10)_t$ plane since it is not a lattice vector nor does it connect the centers of two atoms. The arrangement of the atoms, using a hard sphere model, over the first-order prism plane is shown in Fig. 9 as discussed by Rosenbaum (43). Slip along $[\bar{1}\bar{1}\bar{1}]$ or $\vec{c} + \vec{a}$ may involve atomic movements in the directions $0 \rightarrow 1 \rightarrow 2 \rightarrow 3 \rightarrow 4$. One may say that a total dislocation $[\bar{1}\bar{1}\bar{1}]_t$ would dissociate into four partial dislocations separated by three faults. Thus, a complete incorporation process may involve two successive $[100]_m$ dislocations. A complete as well as a partial incorporation process is illustrated in Fig. 10. The relative elastic energies of the basal slip dislocation and a hypothetical partial dislocation $1/2[111]$ have been calculated to be 3.11 : 2.10 (see Table 3). Furthermore, an $1/2[111]$ or $1/2(\vec{c} + \vec{a})$ dislocation is likely to be in a dissociated state with the partial dislocations discussed before since the resultant vector subtends obtuse angle in the vector triangle in Fig. 9, using the criterion of the square of magnitude of the Burgers vector. Therefore, the dislocation reaction described in Fig. 10 is not impossible.

One can write the dislocation reaction (2) as

$$2 \times [100]_m \longrightarrow [\bar{1}\bar{1}\bar{1}]_t \qquad (3\text{-}1)$$

where $[\bar{1}\bar{1}\bar{1}]_t$ is an extended dislocation as discussed above. One may also say that each basal dislocation $[100]_m$ is an extended one with its partials of Burgers vector $\vec{p}$ (40). The reaction described by (3) is crystallographically equivalent to the reaction (2). By analogy, one can write

$$2 \times [010]_m \longrightarrow [\bar{1}\bar{1}1]_t \qquad (3\text{-}2)$$

In the reactions (2) and (3) what happens at the coherent twin boundary can be expressed by the amount of the twin shear $2\vec{b}_t$ applied to the original vectors. This vector $2\vec{b}_t$ may be called a double twin dislocation as suggested by Thompson and Millard (9) or a zonal twin dislocation (44). Its magnitude is $2b_t = 0.176\ a$, twice as large as that of the unit twin dislocation. This double twin dislocation signifies a step formed at the coherent twin boundary due to the incorporation of slip dislocations. The role played by the double twin dislocations in the process of twin growth and untwinning will be discussed in Sec. 4.

3.3. Incorporation process (4) and (5)

The dislocation reaction for the incorporation process (4) can be written as

$$[11\bar{1}]_m \longrightarrow 2 \times [0\bar{1}0]_t \qquad (3\text{-}3)$$

which resembles Eq. (3-2) in reverse except the interchange of the matrix and the twin. However, the nature of the dislocations involved is very much different from that discussed in Sec. 3.2. The original slip dislocation considered here is a second-order pyramidal slip

dislocation which lies in $(112)_m$. The product $[0\bar{1}0]_t$ lies, according to Table 5, in the first-order prism plane $(\bar{1}00)_t$. Eventhough the basal plane $(001)_t$, the first-order pyramidal plane $(011)_t$, and the first-order prism plane belong to the same zone of crystallographic planes with $[010]_t$ as the zone axis, the portion of the dislocation line incorporated is in the mixed orientation so that it can probably glide only on $(\bar{1}00)_t$ at the beginning of the incorporation process.

The relative elastic energies of a total second-order pyramidal slip dislocation and a pair of first-order prismatic slip dislocations are 9.79 : 2(3.97) = 7.94 (see Table 3). Therefore, the reaction described by Eq. (3-3) is energetically feasible. The slip vector [111] or $\vec{c} + \vec{a}$ is considered to be split in the second-order pyramidal plane into partial dislocations whose Burgers vector is $\vec{p} + 1/2\,\vec{c}$ (40). According to Rosenbaum (43), each partial may dissociate into two other partials. Thus, $[11\bar{1}]_m$ may be an extended dislocation with four partials separated by three faults. By analogy, one can write for the reaction (5)

$$[111]_m \longrightarrow 2 \times [\bar{1}00]_t \qquad (3\text{-}4)$$

In Fig. 11 a schematic illustration is given for the incorporation process (4).

4. Process of twin growth

The effect of the incorporation of slip dislocation at the coherent twin boundary on the growth and untwinning of the existing twins was discussed by Sleeswyk and Verbraak (10) for the body-centered

cubic structure. The following is an extension of their theory to hexagonal zinc crystals.

Take an ideal case that an $(1\bar{1}02)[1\bar{1}0\bar{1}]$ twin is introduced into a zinc crystal of $(11\bar{2}0)[1\bar{1}00]$ orientation as shown in Fig. 12. If a hypothetical pure edge dislocation with an $1/2[1\bar{1}00]_m$ Burgers vector is forced to glide in the basal plane of the matrix and in the first-order prism plane of the twin by the applied shear stress as indicated in Fig. 12, the net effect would be to cause the portion of the crystal above the slip traces to glide to the left by $1/2[1\bar{1}00]$ with respect to the portion below. A step will be formed at each of the two interfaces. Each step is in fact a twin dislocation since it separates the twinned region from the matrix. Whether the twin will grow or shrink depends upon the direction of the shear stress applied to these twin dislocations. The shear stress shown in Fig. 12 will cause the twin to grow by one twin layer as the twin dislocations are forced to glide to the free surfaces. Reversing the direction of the applied shear stress will cause the twin to shrink by one twin layer.

The effect of an actual basal slip dislocation $1/3[2\bar{1}\bar{1}0]_m$ may be considered as the equivalent of the combined effects of the edge component $1/2[1\bar{1}00]_m$ as discussed above and the screw component $1/6[11\bar{2}0]_m$. The latter is parallel to the coherent twin boundary and has no effect on the twin other than causing the upper portion of the crystal to glide in the direction normal to the plane of drawing by $1/6[11\bar{2}0]$ with respect to the lower portion.

When the surfaces in Fig. 12 are restrained or in an actual case that the stress field in the neighborhood of the twinned region

resists the change in shape and volume of the twin, the net effect will be equivalent to forcing the dotted line contour to coincide with the solid line contour in Fig. 12. This action will cause the twinned region at A to untwin and the region of the matrix at B to twin. In other words, a pair of twin dislocations of opposite sign is formed at each coherent twin boundary as shown in Fig. 13. Under the applied shear stress as indicated the pair at B will annihilate each other, whereas the pair at A will move away from each other and cause the twin to grow by one twin layer over the area swept by this pair of twin dislocations. Reversing the direction of the shear stress acting on these twin dislocations, the pair at A will annihilate each other whereas the pair at B will move away from each other causing the existing twin to untwin by one twin layer. Thus, whether the resulting effect is to cause the twin to grow or to shrink depends only upon the direction of the applied shear stress.

In the above, twin growth resulting from the incorporation of slip dislocations at the coherent twin boundary has been discussed without questioning the mobility of the resulting dislocations in the twin after the incorporation process. For instance there has been no experimental evidence of an active slip system with a $<\vec{c}+\vec{a}>$ slip vector on the first-order prism plane in zinc. The calculation of the degree of ease of gliding of six potential slip systems in zinc shows that prismatic slip in the diagonal direction is the second hardest one next only to the "normal slip" with the slip vector $\vec{c}$ (see Table 3). Prismatic slip in the close-packed direction was observed by Gilman (45)

in zinc only at elevated temperatures of 250 ~ 400°C. The calculation also shows that this slip system ranks fourth in the relative ease of gliding next to basal, second-order pyramidal, and first-order pyramidal slips. Thus, unlike the case of the body-centered cubic lattice as discussed by Sleeswyk and Verbraak,the reaction product described in (2) or (3), a prismatic slip dislocation with a $<\vec{c}+\vec{a}>$ Burgers vector, would not probably glide to any great extent on the prism plane. Subsequent dislocations in the matrix may form a pile-up against the coherent twin boundary and produce a region of stress concentration. This stress concentration may indeed facilitate the dislocation incorporation process by forcing the reaction product to glide on the unfavorable slip plane over a short distance, and then its screw portion may cross glide onto the second-order pyramidal plane. Similarly, the reaction product described in (4) and (5), a prismatic slip dislocation with Burgers vector $<\vec{a}>$, would probably glide only over a limited extent on the prism plane at room temperature, but its screw portion may cross glide onto the basal plane.

The incorporation of the other second-order pyramidal slip dislocations described in (6) through (9) of Table 4 is not likely to take place for the reasons mentioned previously. These dislocations may, however, pile up against the coherent twin boundary and may even cause new twins to be nucleated.

Some combinations of the incorporation processes discussed above may possibly take place. For instance, an association of a dislocation with the Burgers vector $\vec{c}+\vec{a}$ and another with $-\vec{a}$ aided

by a stress concentration will give a dislocation with the Burgers vector $\vec{c}$, which may be incorporated at the coherent twin boundary to produce a double twin dislocation $2\vec{b}_t$ and a $[-\vec{a}'_1 + \vec{a}'_2]_t$ dislocation in the twin as described in (10) of Table 4.

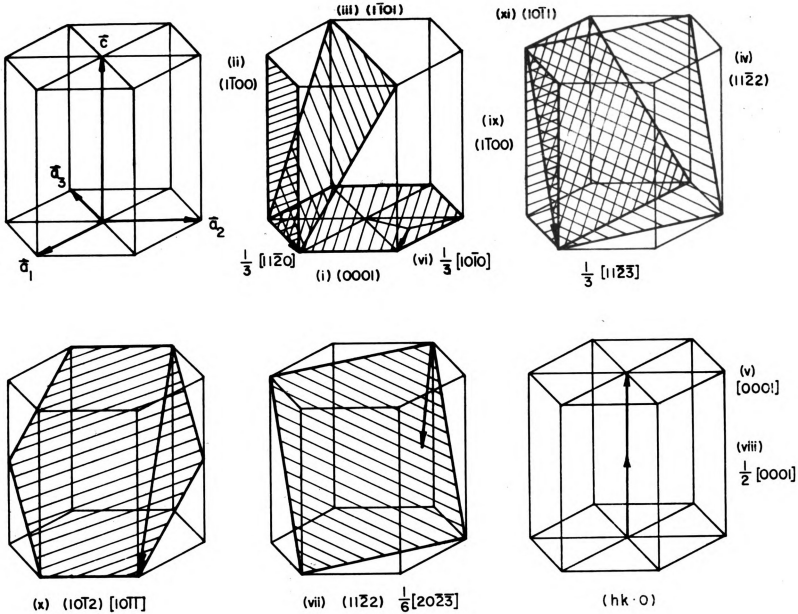

Figure 1. Slip systems and twin system in zinc crystal.

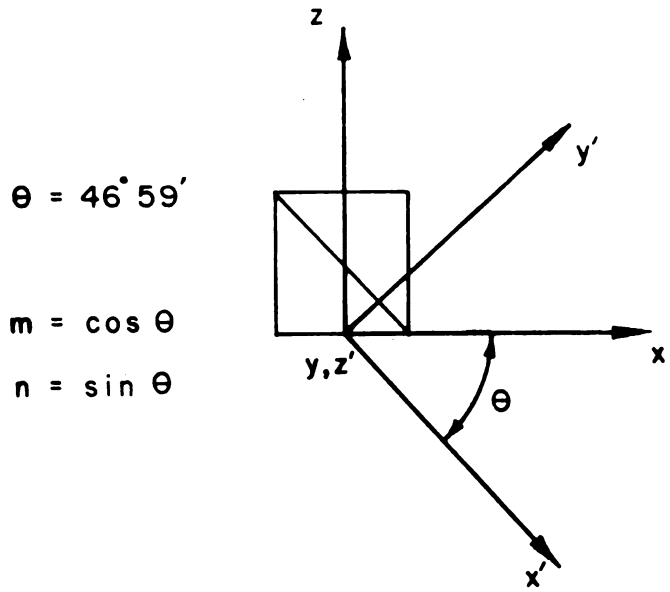

	x	y	z
x'	m	0	-n
y'	n	0	m
z'	0	-1	0

Figure 2. Coordinate transformation for $\{10\bar{1}2\}\ \langle 10\bar{1}\bar{1}\rangle$ twin system; y and z' axes coincide both perpendicular to the plane of drawing.

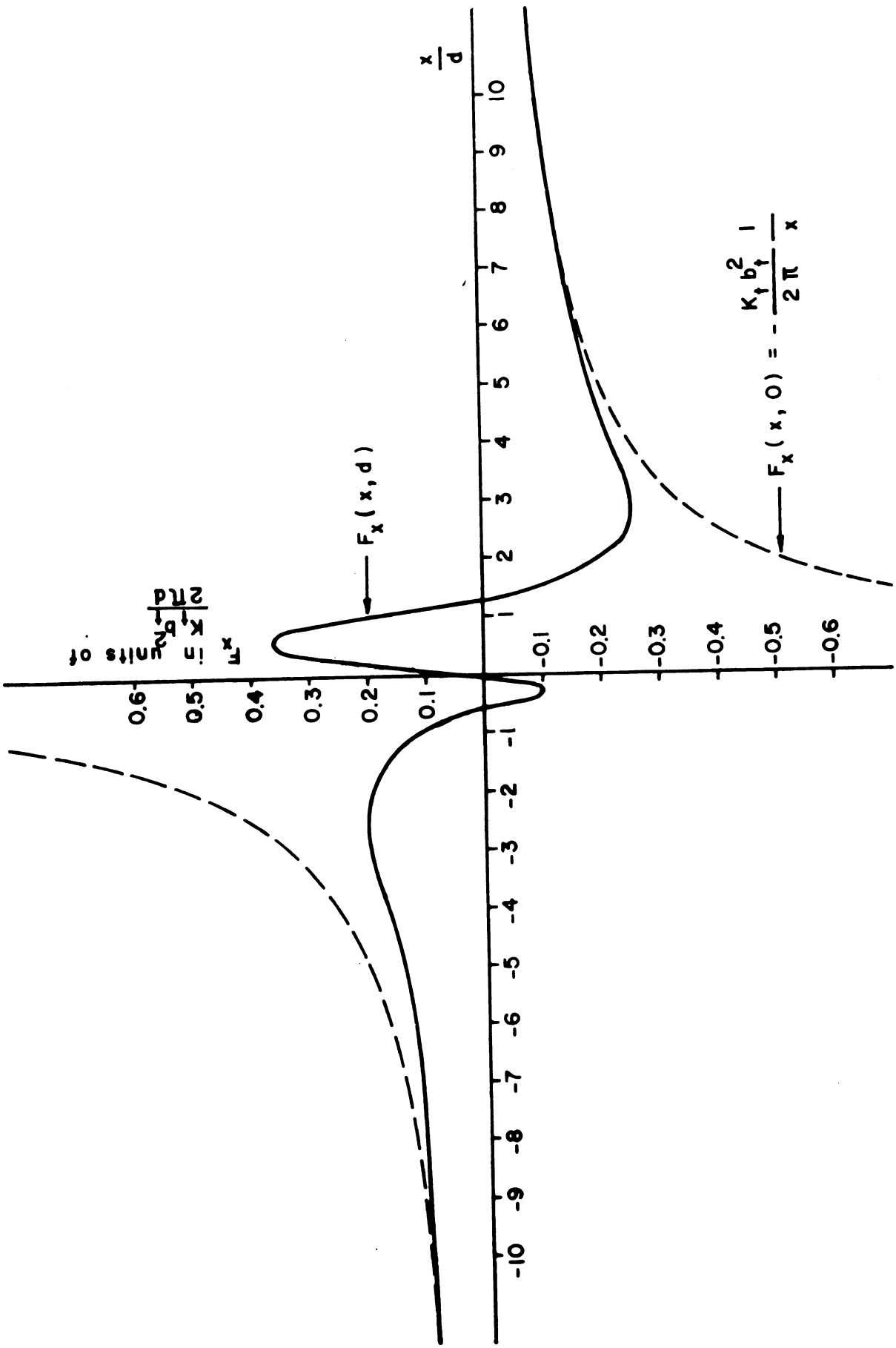

Figure 3. Interaction forces between two parallel twin dislocations in the edge orientation, x-component.

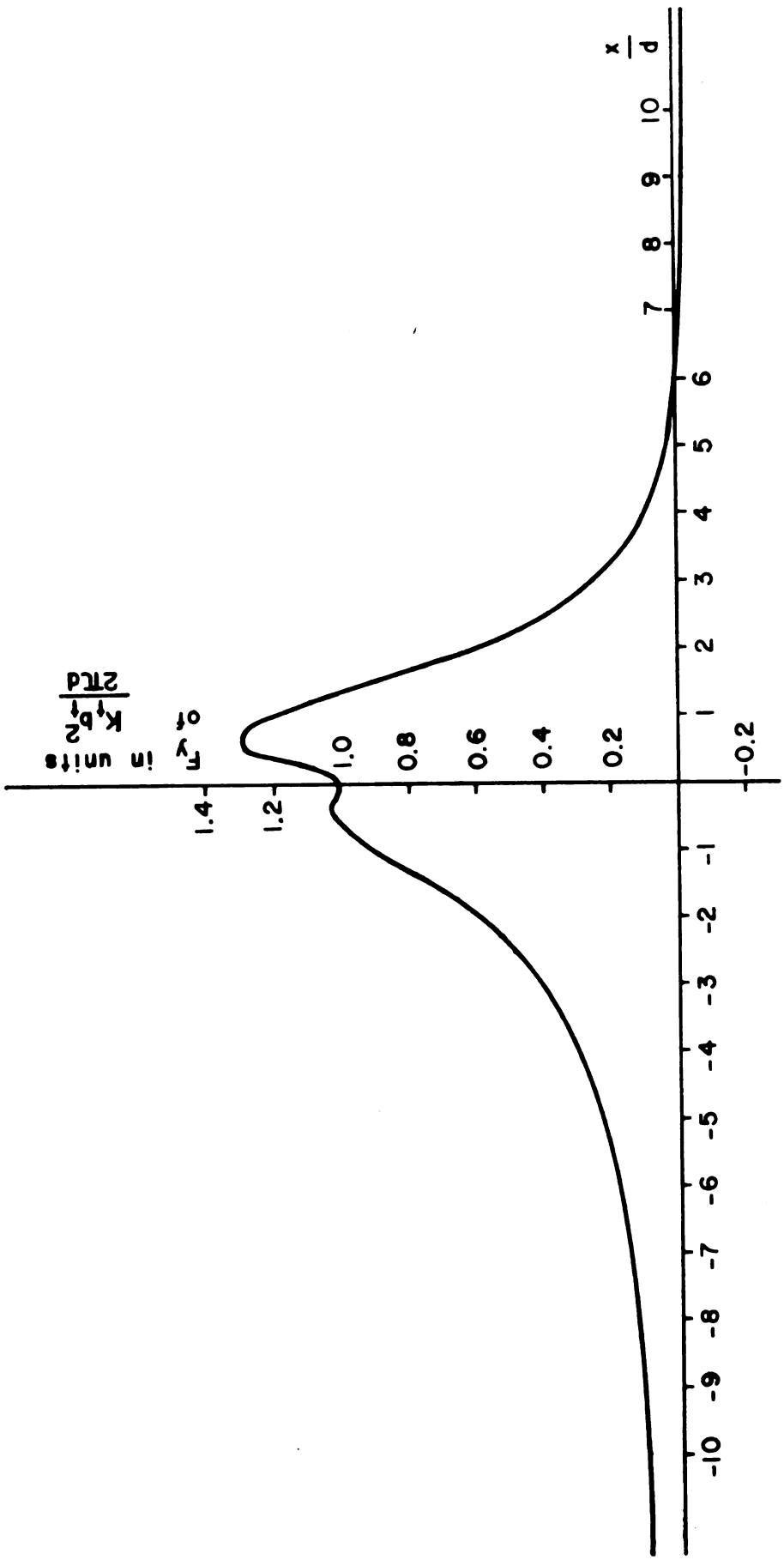

Figure 4. Interaction forces between two parallel twin dislocations in the edge orientation, y-component.

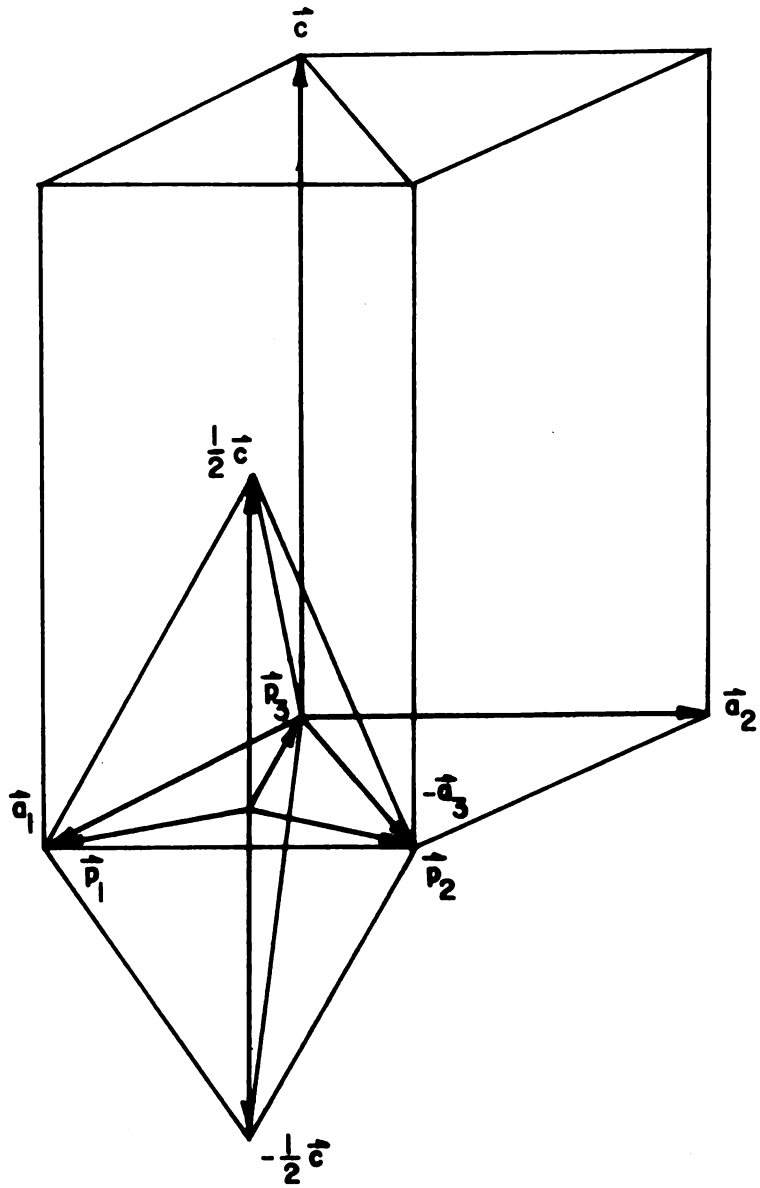

Figure 5. Burgers vectors in hexagonal close-packed lattice.

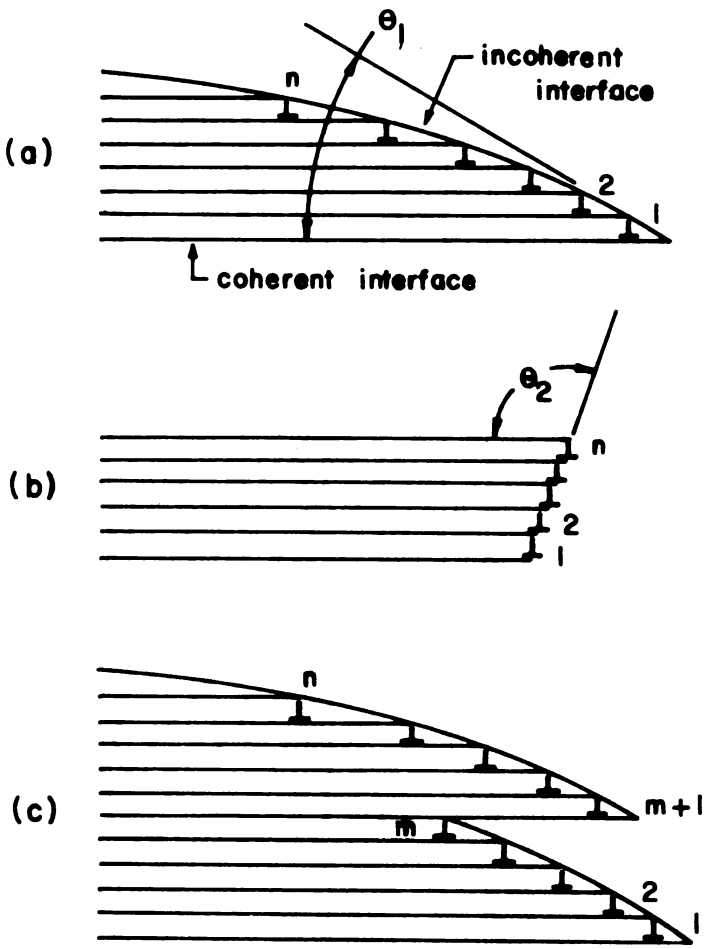

Figure 6. Possible shapes of twin boundaries in zinc crystals.

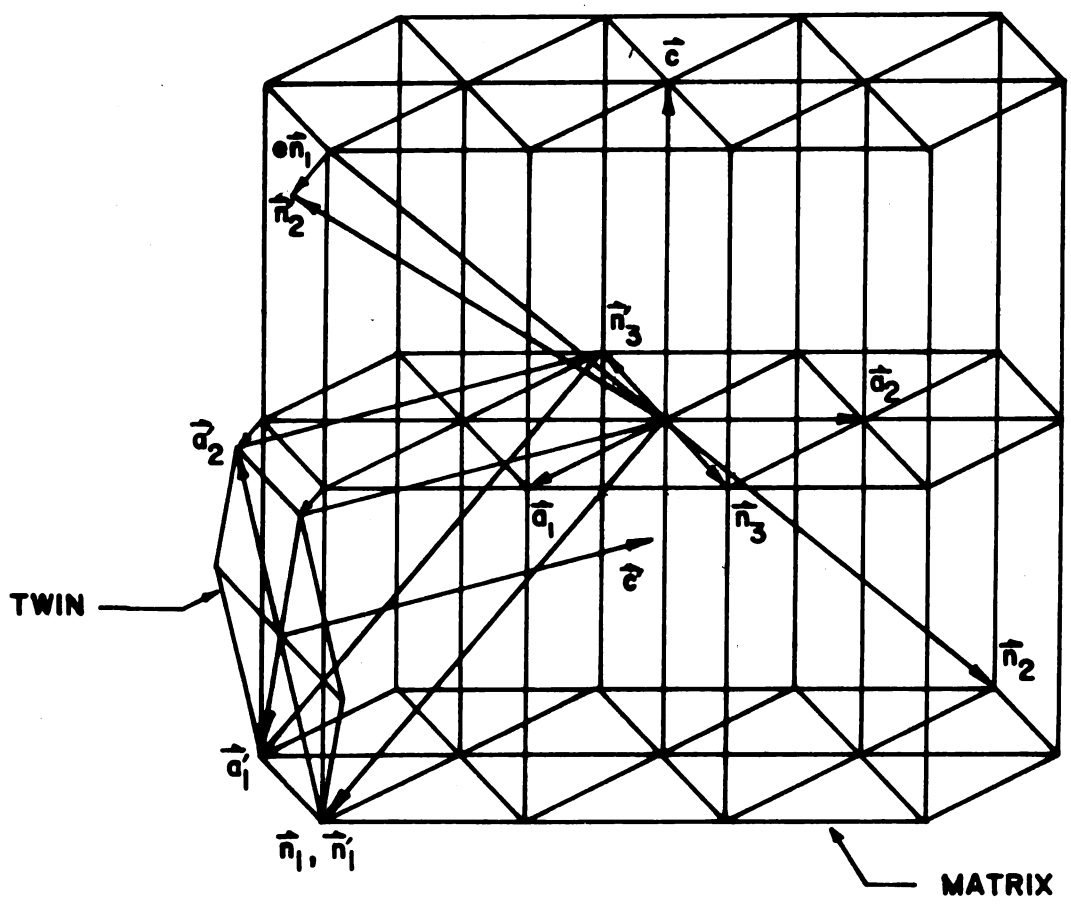

Figure 7. Base vectors of the coordinate systems used for transformation of the Burgers vectors of slip dislocations.

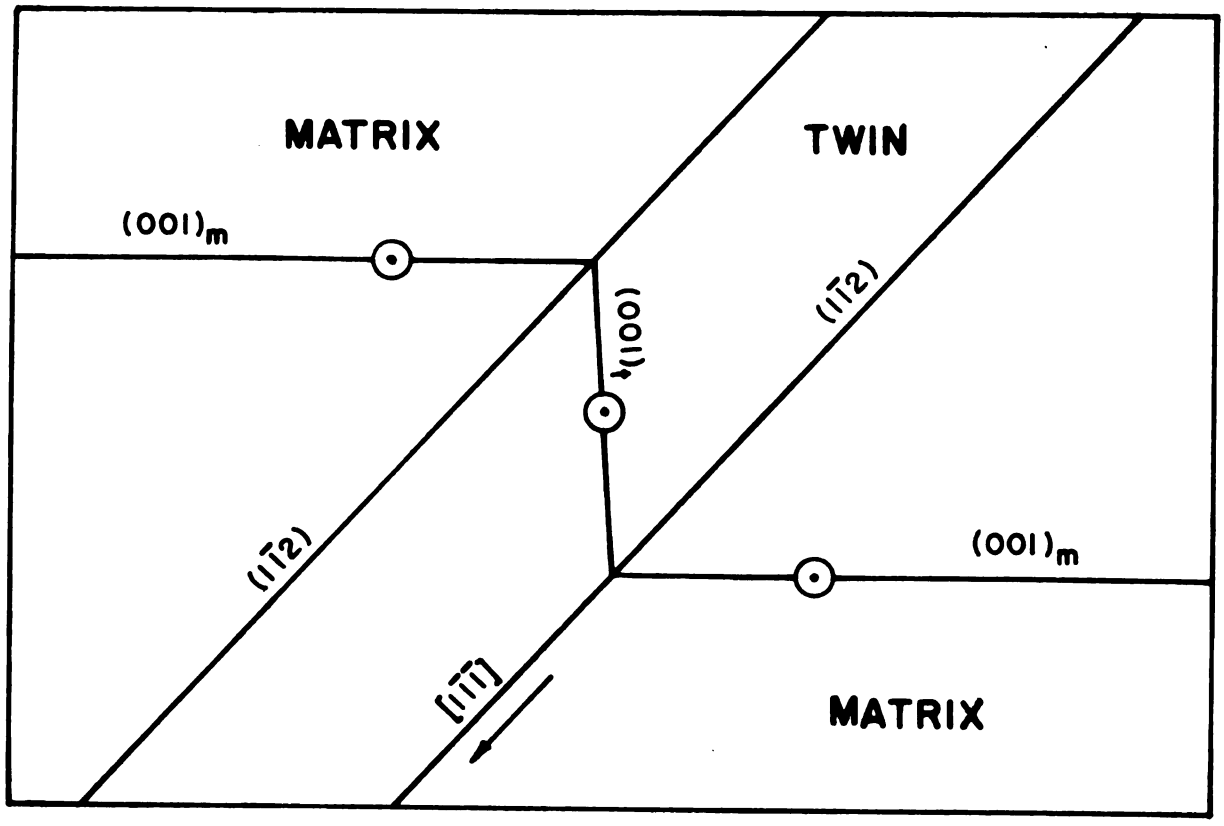

Figure 8. Incorporation of $[\,110]_m$ slip dislocation in the $(1\bar{1}2)[\,1\bar{1}\bar{1}]$ twin. ⊙ represents a pure screw dislocation with the Burgers vector normal to and outward from the plane of drawing (110).

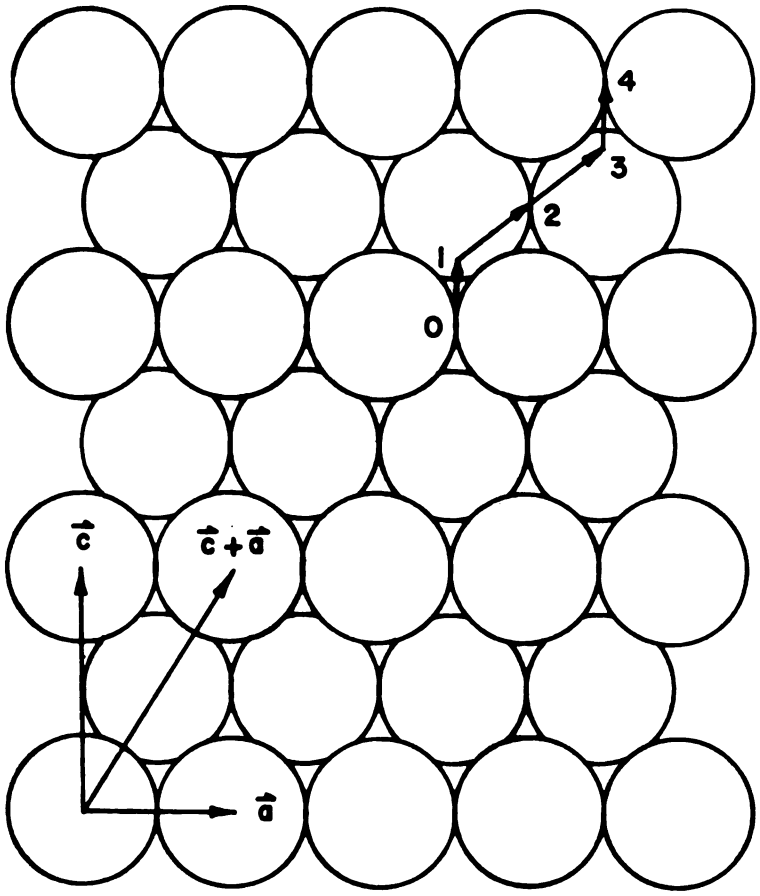

Figure 9. First-order prism plane of hexagonal close-packed structure of hard spheres.

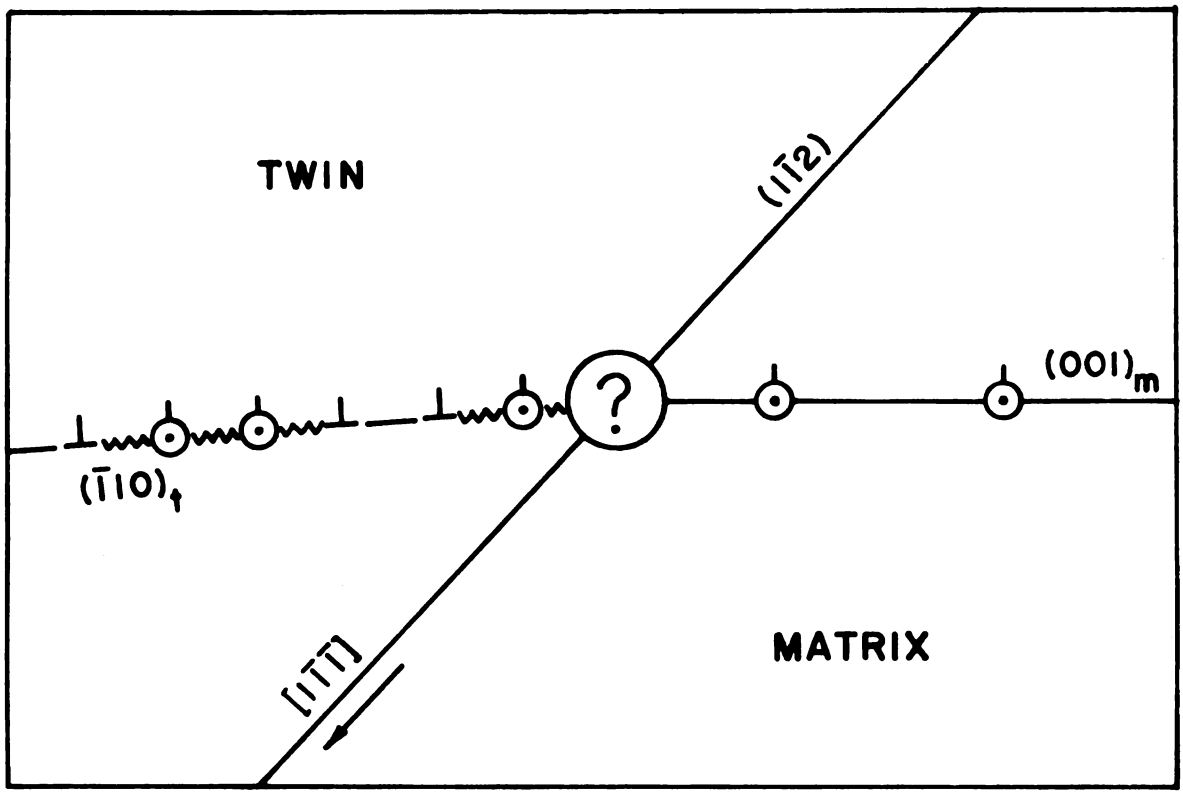

Figure 10. Incorporation of $[100]_m$ slip dislocation in the $(1\bar{1}2)[1\bar{1}\bar{1}]$ twin. $\perp$ and $\dot{o}$ represent a pure edge and a mixed dislocation respectively. $\cdot\checkmark$ represents a stacking fault. Plane of drawing is (110).

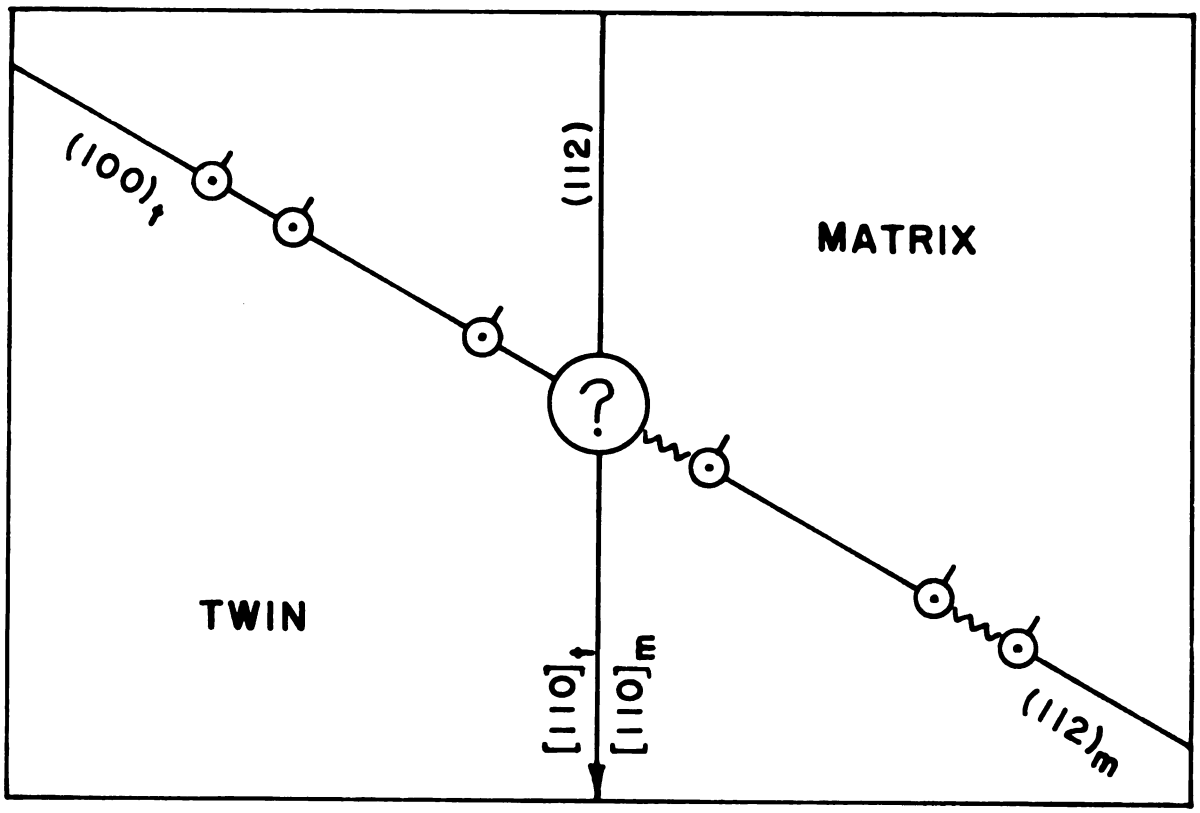

Figure 11. Incorporation of $[11\bar{1}]_m$ slip dislocation in the $(1\bar{1}2)[1\bar{1}1]$ twin. Plane of drawing is nearly $(\bar{1}12)$.

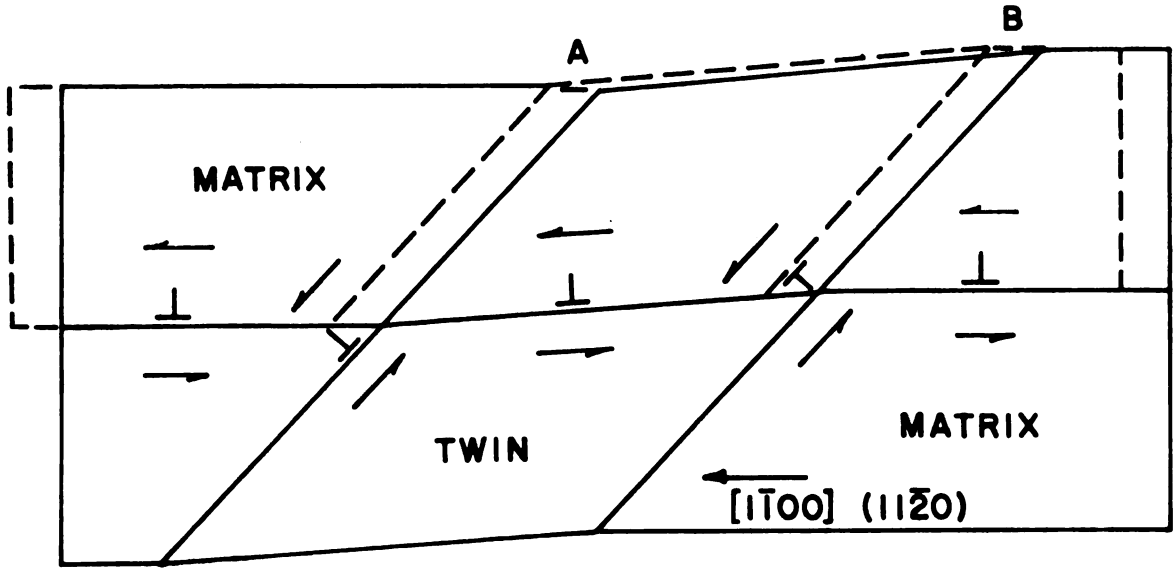

Figure 12. Twin growth by incorporation of a slip dislocation in the absence of surface restraints.

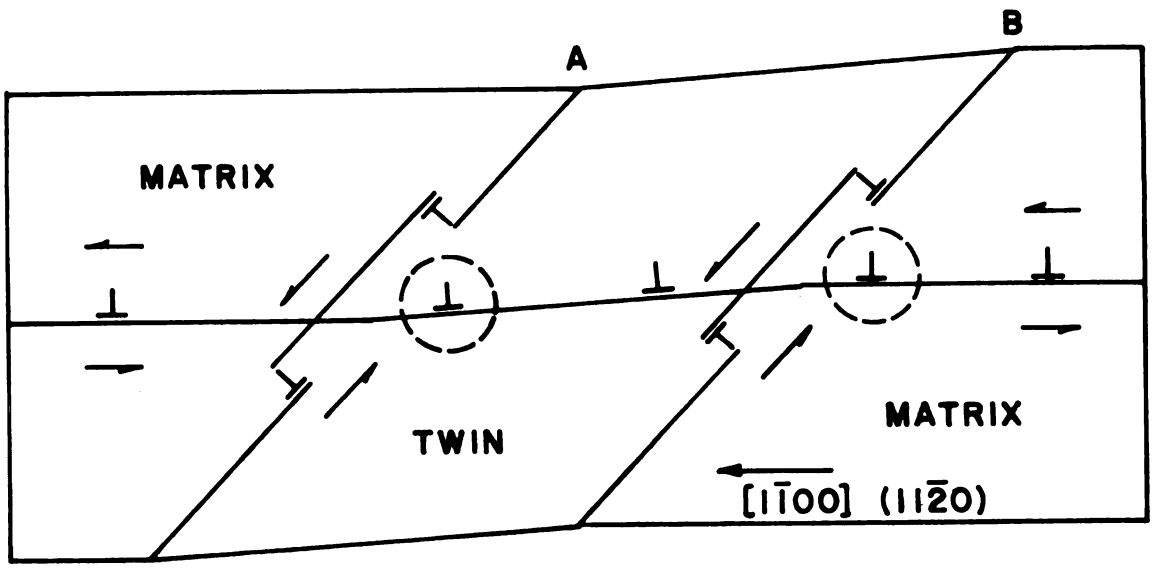

Figure 13. Twin growth by incorporation of a slip dislocation in the presence of surface restraints.

Table 2. Transformed elastic constants and K for edge dislocations

Slip System	Direction Cosines of Trans. a_{ij}	$C'_{ij} \times 10^{-11}$ (dynes/cm^2)	$S'_{ij} \times 10^{12}$ (cm^2/dyne)	$S^*_{ij} \times 10^{12}$ (i, j=1, 2, 6) (cm^2/dyne)	$K \times 10^{-11}$ (dynes/cm^2)
(i) basal slip (vi) {0001} <11$\bar{2}$0> or <hk.0>	$\begin{pmatrix} 1 & 0 & 0 \\ 0 & 0 & 1 \\ 0 & -1 & 0 \end{pmatrix}$ $\theta = 90^\circ$	$\begin{matrix} 16.10 & 5.01 & 3.35 & 0 & 0 & 0 \\ & 6.10 & 5.01 & 0 & 0 & 0 \\ & & 16.10 & 0 & 0 & 0 \\ & & & 3.83 & 0 & 0 \\ & & & & 6.38 & 0 \\ & & & & & 3.83 \end{matrix}$	$\begin{matrix} .84 & -.73 & .05 & 0 & 0 & 0 \\ & 2.84 & -.73 & 0 & 0 & 0 \\ & & .84 & 0 & 0 & 0 \\ & & & 2.61 & 0 & 0 \\ & & & & 1.57 & 0 \\ & & & & & 2.61 \end{matrix}$	$\begin{matrix} .84 & -.69 & 0 \\ & 2.20 & 0 \\ & & 2.61 \end{matrix}$	5.51
(ii) prismatic slip {1$\bar{1}$00} <11$\bar{2}$0>	$\begin{pmatrix} 1 & 0 & 0 \\ 0 & 1 & 0 \\ 0 & 0 & 1 \end{pmatrix}$ $\theta = 0^\circ$	$\begin{matrix} 16.10 & 3.35 & 5.01 & 0 & 0 & 0 \\ & 16.10 & 5.01 & 0 & 0 & 0 \\ & & 6.10 & 0 & 0 & 0 \\ & & & 3.83 & 0 & 0 \\ & & & & 3.83 & 0 \\ & & & & & 6.38 \end{matrix}$	$\begin{matrix} .84 & .05 & -.73 & 0 & 0 & 0 \\ & .84 & .05 & 0 & 0 & 0 \\ & & 2.84 & 0 & 0 & 0 \\ & & & 2.61 & 0 & 0 \\ & & & & 2.61 & 0 \\ & & & & & 1.57 \end{matrix}$	$\begin{matrix} .65 & -.14 & 0 \\ & .65 & 0 \\ & & 1.57 \end{matrix}$	7.70
(iii) 1st order pyramidal slip {1$\bar{1}$01} <11$\bar{2}$0>	$\begin{pmatrix} 1 & 0 & 0 \\ 0 & m & -n \\ 0 & n & m \end{pmatrix}$ $\theta = 25^\circ 3'$	$\begin{matrix} 16.10 & 3.65 & 4.71 & -.64 & 0 & 0 \\ & 14.77 & 4.55 & 1.53 & 0 & 0 \\ & & 8.35 & 2.30 & 0 & 0 \\ & & & 3.37 & 0 & 0 \\ & & & & 4.29 & 0 \\ & & & & & 5.92 \end{matrix}$	$\begin{matrix} .84 & -.09 & -.51 & -.60 & 0 & 0 \\ & .83 & -.36 & -.15 & 0 & 0 \\ & & 2.11 & -1.39 & 0 & 0 \\ & & & 4.10 & 0 & 0 \\ & & & & 2.42 & -.40 \\ & & & & & 1.76 \end{matrix}$	$\begin{matrix} .72 & -.14 & 0 \\ & .72 & 0 \\ & & 1.69 \end{matrix}$	7.02*
(iv) 2nd order pyramidal slip {11$\bar{2}$2} <11$\bar{2}$3>	$\begin{pmatrix} m & 0 & -n \\ n & 0 & m \\ 0 & -1 & 0 \end{pmatrix}$ $\theta = 61^\circ 41' 14''$	$\begin{matrix} 8.90 & 4.46 & 4.64 & 0 & 0 & 2.45 \\ & 14.40 & 3.72 & 0 & 0 & 1.73 \\ & & 16.10 & 0 & 0 & -.69 \\ & & & 5.81 & 1.06 & 0 \\ & & & & 4.40 & 0 \\ & & & & & 3.28 \end{matrix}$	$\begin{matrix} 1.95 & -.29 & -.56 & 0 & 0 & -1.42 \\ & .85 & -.12 & 0 & 0 & -.25 \\ & & .84 & 0 & 0 & .66 \\ & & & 1.80 & -.43 & 0 \\ & & & & .238 & 0 \\ & & & & & 4.37 \end{matrix}$	$\begin{matrix} 1.58 & -.37 & -.98 \\ & .83 & -.16 \\ & & 3.86 \end{matrix}$	3.90

*Approximate values

Table 2. (continued)

Slip System	Direction Cosines of Trans. a_{ij}	$C'_{ij} \times 10^{-11}$ (dynes/cm^2)	$S'_{ij} \times 10^{12}$ (cm^2/dyne)	$S^*_{ij} \times 10^{12}$ (i, j=1, 2, 6) (cm^2/dyne)	$K \times 10^{-11}$ (dynes/cm^2)
(x) mechanical twinning $\{10\bar{1}2\}$ $<10\bar{1}\bar{1}>$	$\begin{pmatrix} m & 0 & -n \\ n & 0 & m \\ 0 & -1 & 0 \end{pmatrix}$ $\theta = 46^\circ 59'$	$\begin{pmatrix} 11.53 & 4.23 & 4.24 & 0 & 0 & 2.55 \\ & 12.23 & 4.12 & 0 & 0 & 2.44 \\ & & 16.10 & 0 & 0 & -.83 \\ & & & 5.19 & 1.27 & 0 \\ & & & & 5.02 & 0 \\ & & & & & 3.04 \end{pmatrix}$	$\begin{pmatrix} 1.28 & -.10 & -.36 & 0 & 0 & -1.09 \\ & 1.14 & -.31 & 0 & 0 & -.91 \\ & & .84 & 0 & 0 & .78 \\ & & & 2.05 & -.52 & 0 \\ & & & & 2.13 & 0 \\ & & & & & 5.13 \end{pmatrix}$	$\begin{pmatrix} 1.12 & -.24 & -.75 \\ & 1.02 & -.62 \\ & & 4.40 \end{pmatrix}$	4.08
(v), (viii) $\{hk.0\}$ $<0001>$	$\begin{pmatrix} 0 & 0 & -1 \\ -1 & 0 & 0 \\ 0 & 1 & 0 \end{pmatrix}$ $\theta = 90^\circ$	$\begin{pmatrix} 6.10 & 5.01 & 5.01 & 0 & 0 & 0 \\ & 16.10 & 3.35 & 0 & 0 & 0 \\ & & 16.10 & 0 & 0 & 0 \\ & & & 6.38 & 0 & 0 \\ & & & & 3.83 & 0 \\ & & & & & 3.83 \end{pmatrix}$	$\begin{pmatrix} 2.84 & -.73 & -.73 & 0 & 0 & 0 \\ & .84 & .05 & 0 & 0 & 0 \\ & & .84 & 0 & 0 & 0 \\ & & & 1.57 & 0 & 0 \\ & & & & 2.61 & 0 \\ & & & & & 2.61 \end{pmatrix}$	$\begin{pmatrix} 2.20 & -.69 & 0 \\ & .84 & 0 \\ & & 2.61 \end{pmatrix}$	3.39
(vii) $\{11\bar{2}2\}$ $<20\bar{2}\bar{3}>$	$\begin{pmatrix} m & 0 & -n \\ n & 0 & m \\ 0 & -1 & 0 \end{pmatrix}$ $\theta = 46^\circ 23' 15''$	$\begin{pmatrix} 11.64 & 4.23 & 4.22 & 0 & 0 & 2.53 \\ & 12.12 & 4.14 & 0 & 0 & 2.46 \\ & & 16.10 & 0 & 0 & -.83 \\ & & & 5.17 & 1.27 & 0 \\ & & & & 5.04 & 0 \\ & & & & & 3.05 \end{pmatrix}$	$\begin{pmatrix} 1.23 & -.10 & -.36 & 0 & 0 & -1.06 \\ & 1.16 & -.32 & 0 & 0 & -.94 \\ & & .84 & 0 & 0 & .78 \\ & & & 2.07 & -.52 & 0 \\ & & & & 2.12 & 0 \\ & & & & & 5.13 \end{pmatrix}$	$\begin{pmatrix} 1.10 & -.24 & -.73 \\ & 1.04 & -.64 \\ & & 4.40 \end{pmatrix}$	4.13*
(ix) $\{1\bar{1}00\}$ $<11\bar{2}\bar{3}>$	$\begin{pmatrix} m & 0 & n \\ 0 & 1 & 0 \\ -n & 0 & m \end{pmatrix}$ $\theta = 61^\circ 14' 41''$	$\begin{pmatrix} 8.90 & 4.64 & 4.46 & 0 & -2.45 & 0 \\ & 16.10 & 3.72 & 0 & .69 & 0 \\ & & 14.40 & 0 & -1.73 & 0 \\ & & & 5.81 & 0 & -1.06 \\ & & & & 3.28 & 0 \\ & & & & & 4.40 \end{pmatrix}$	$\begin{pmatrix} 1.95 & -.56 & -.29 & 0 & 1.42 & 0 \\ & .84 & -.12 & 0 & -.66 & 0 \\ & & .85 & 0 & .25 & 0 \\ & & & 1.80 & 0 & .43 \\ & & & & 4.37 & 0 \\ & & & & & 2.38 \end{pmatrix}$	$\begin{pmatrix} 1.56 & -.48 & 0 \\ & .77 & 0 \\ & & 2.27 \end{pmatrix}$	4.28*

*Approximate values

Table 3. Elastic properties of edge dislocations in zinc crystals.

slip system	(1) slip plane y=0	(2) slip direction x	(3) Burgers vector b	(4) b	(5) spacing between slip planes d	(6) inverse of shear strain d/b	(7) $C'_{66} \times 10^{-11}$ (dynes/cm^2)
(i) basal (total)	(0001)	$[11\bar{2}0]$	$1/3[11\bar{2}0]$	a	.928 a	.928	3.83
(ii) prismatic (close-packed direction)	$(1\bar{1}00)$	$[11\bar{2}0]$	$1/3[11\bar{2}0]$	a	.577 a	.577	6.38
(iii) pyramidal 1st order	$(1\bar{1}01)$	$[11\bar{2}0]$	$1/3[11\bar{2}0]$	a	.655 a	.655	5.92
(iv) pyramidal 2nd order	$(11\bar{2}2)$	$[11\bar{2}\bar{3}]$	$1/3[11\bar{2}\bar{3}]$	2.108 a	.440 a	.209	3.28
(v) normal (total)	(hk.0)	[0001]	[0001]	1.856 a	.577 a	.311	3.83
(vi) basal (partial)	(0001)	$[10\bar{1}0]$	$1/3[10\bar{1}0]$	.577 a	.928 a	1.608	3.83
(vii) pyramidal 2nd order (partial)	$(11\bar{2}2)$	$[20\bar{2}\bar{3}]$	$1/6[20\bar{2}\bar{3}]$	1.093 a	.440 a	.403	3.05
(viii) normal (partial)	(hk.0)	[0001]	1/2[0001]	.928 a	.577 a	.622	3.83
(ix) prismatic (diagonal)	$(1\bar{1}00)$	$[11\bar{2}\bar{3}]$	$1/6[11\bar{2}\bar{3}]$	1.054 a	.577 a	.547	4.40
(x) twin	$(10\bar{1}2)$	$[10\bar{1}\bar{1}]$	$t[10\bar{1}\bar{1}]$	.088 a	.633 a	7.193	3.04

c = 4.9468 Å
a = 2.6649 Å

$\frac{c}{a} = 1.856$

isotropy ($\nu = 1/3$) $K = \frac{\mu}{1-\nu} = 5.58 \times 10^{11}$ dynes/cm^2

Table 3 (continued)

slip system	(8) $K \times 10^{-11}$ (dynes/cm^2)	(9) $S'_{66} \times 10^{12}$ (cm^2/dyne)	(10) $\frac{E}{\ln(R/r_o)} \times 10^5$ (ergs/cm)	(11) ζ	(12) degree of ease of gliding ζ/b	(13) sequence in ease of gliding
(i) basal (total)	5.51	2.61	3.11	.667 a	.667	
(ii) prismatic (close-packed direction)	7.70	1.57	4.35	.349 a	.349	4
(iii) pyramidal 1st order	7.02*	1.76	3.97	.405 a	.405	3
(iv) pyramidal 2nd order	3.90	4.37	9.79	.375 a	.179	
(v) normal (total)	3.39	2.61	6.43	.511 a	.138	
(vi) basal (partial)	5.51	2.61	1.04	.667 a	1.156	1
(vii) pyramidal 2nd order (partial)	4.13*	5.13	2.79	.466 a	.428	2
(viii) normal (partial)	3.39	2.61	1.61	.511 a	.275	6
(ix) prismatic diagonal	4.28*	2.38	2.10	.294 a	.278	5
(x) twin	4.08	5.13	.018	.633 a		

*Approximate value

Table 4. Transformation of Burgers Vectors

	$\underline{X}$	$\underline{X}^* = \underline{X}\,\underline{T}^*$	$\underline{X}^* - \underline{X}' = \underline{X}\,\underline{B}$
(1)	$\pm[110]_m$	$\pm[\bar{1}\bar{1}0]_t$	$[000]$
(2)	$\pm[100]_m$	$\pm\frac{1}{2}[\bar{1}\bar{1}\bar{1}]_t$	$\pm\frac{1}{4}\,e[1\bar{1}\bar{1}] = \pm\vec{b}_t$
(3)	$\pm[010]_m$	$\pm\frac{1}{2}[\bar{1}\bar{1}1]_t$	$\pm\frac{1}{4}\,e[\bar{1}11] = \mp\vec{b}_t$
(4)	$\pm[11\bar{1}]_m$	$\pm 2[0\bar{1}0]_t$	$\pm\frac{1}{2}\,e[\bar{1}11] = \mp 2\vec{b}_t$
(5)	$\pm[111]_m$	$\pm 2[\bar{1}00]_t$	$\pm\frac{1}{2}\,e[1\bar{1}\bar{1}] = \pm 2\vec{b}_t$
(6)	$\pm[10\bar{1}]_m$	$\pm\frac{1}{2}[\bar{1}3\bar{1}]_t$	$\pm\frac{1}{4}\,e[\bar{1}11] = \mp\vec{b}_t$
(7)	$\pm[011]_m$	$\pm\frac{1}{2}[\bar{3}11]_t$	$\pm\frac{1}{4}\,e[1\bar{1}\bar{1}] = \pm\vec{b}_t$
(8)	$\pm[01\bar{1}]_m$	$\pm\frac{1}{2}[1\bar{3}1]_t$	$\pm\frac{3}{4}\,e[\bar{1}11] = \mp 3\vec{b}_t$
(9)	$\pm[101]_m$	$\pm\frac{1}{2}[\bar{3}1\bar{1}]_t$	$\pm\frac{3}{4}\,e[1\bar{1}\bar{1}] = \pm 3\vec{b}_t$
(10)	$\pm[001]_m$	$\pm[\bar{1}10]_t$	$\pm\frac{1}{2}\,e[\bar{1}11] = \mp 2\vec{b}_t$

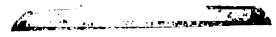

Table 5. Transformation of Slip Planes

	$(hkl)_m$		$(HKL)_t$	
(1)(2)(3)	$(001)_m$	basal	$(\bar{1}10)_t$	prismatic (1st-order)
(4)	$(112)_m$	pyramidal (2nd-order)	$(\bar{1}00)_t$	prismatic (1st-order)
(5)	$(11\bar{2})_m$		$(0\bar{1}0)_t$	
(6)	$(\bar{2}1\bar{2})_m$		$(3\bar{1}6)_t$	high index plane
(7)	$(\bar{1}2\bar{2})_m$		$(1\bar{3}6)_t$	
(8)	$(1\bar{2}\bar{2})_m$		$(3\bar{1}\bar{6})_t$	
(9)	$(2\bar{1}\bar{2})_m$		$(1\bar{3}\bar{6})_t$	
(10)	$(1\bar{1}0)_m$		$(001)_t$	

The factor of 2, due to the double lattice in h. c. p. structure, is omitted for brevity.

III. EXPERIMENTAL PROCEDURES

The purpose of the experimental part of the present work was to find material proof of some, if not all, of the mechanisms described in Chapter II that might account for the growth of existing twins in zinc and to determine, if possible, the resolved shear stresses for the thickening and widening of the twins by using specific loading methods and oriented zinc single crystals.

1. Preparation of the specimens

Zinc single crystals were grown from the melt using zinc of 99.995+ % purity and a modified Bridgeman technique (46). The orientation of the crystals was controlled by welding a seed to the blank so that, after growing, the (0001) plane was parallel to one of the specimen surfaces. The crystals were then cut into various desired dimensions with an acid saw, and chemically polished using a technique suggested by Vreeland et al (47). The orientation and the dimensions of the specimens tested are described in Fig. 14.

2. Methods of loading

2.1. Simple bending

The specimens E, F, and G (see Fig. 14) were simply supported on a bending fixture which was laid on the base plate of a compression load cell in an Instron testing machine. The bending fixture consisted of two knife edges, a stationary one and a movable one, by means of which the beam span could vary from 25 to 76 mm.

Another knife edge was fixed on the crosshead of the testing machine. The downward speed of the crosshead was adjusted to 0.005 cm/min and occasionally to 0.05 cm/min. The knife edges were carefully aligned before each series of testings.

2.2. Uniaxial tension

The specimens E, F, G, and H were cemented to tensile specimen holders by using Armstrong cement. Most of the crystals tested in tension were constricted with approximately 30% reduction in the cross-sectional area over a gage length of 32 mm. The specimens were held by their holders with a pair of jaws attached to the testing machine. A crosshead speed of 0.005 cm/min was selected for the tension tests.

2.3. Point loading

The specimens A, B, C, and D (see Fig. 14) were mounted on the base plate of a compression load cell with a sheet of plastic laid underneath to avoid non-uniform contact between the crystal and the base plate. The downward speed of the crosshead was adjusted to 0.05 cm/min. The load was applied by a pin indenter, which was fixed on the crosshead, in the $[000\bar{1}]$ direction on the (0001) surface of the specimens. Twelve different pin indenters with the radii of their tips ranging from 0.009 to 0.205 mm and the apex angles from 16° to 36° were used.

In all three types of loading, the load vs. crosshead displacement curves were recorded with a pre-calibrated Speedomax recorder.

The appearance and the size of the twins and the slip traces were examined with a Bausch and Lomb Research Metallograph. An intermittent polishing was often given to the specimens between successive tests at increasing load levels.

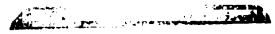

IV. RESULTS

1. Simple bending tests

Six specimens were tested by simple bending with the beam span L = 40 mm. The R.S.S. respectively for the nucleation of twins and the growth of twins are calculated in accordance with the stress analysis described in the Appendix C, and the values for the growth of twins are listed in Table 6. The Eq. (C-4) in the Appendix C can be directly used for the simple bending tests (S.B.) No. 1, 2, 3, and 6. The R.S.S. for twinning in S.B. No. 4 and No. 5 were obtained by a proper transformation of the stress components into their respective twin planes and directions using the Eq's. (C-2) and (C-3).

The specimens in which the basal planes were parallel to the axes of the applied bending moments continued to deform and became unstable on the bending fixture. In S.B. No. 5 no twins were formed by the continuous bending up to the load P = 4.5 kg and the maximum deflection δ_m = 2.1 mm. Basal slip traces were observed on both $(10\bar{1}0)$ edges. The specimen was then bent in the reverse direction up to P = 8.0 kg and δ = - 0.22 mm without forming any twins. When the bending in the original direction was resumed, a twin nucleation took place at P = 5.55 kg and δ = 0.03 mm accompanied by a load drop of approximately 20%. A pair of conjugate twins were observed on one of the $(10\bar{1}0)$ edges, one impinging upon the other. The twin on the other $(10\bar{1}0)$ edge is as shown in Fig. 15, whereas on the (0001) surface, as shown in Fig. 16. In S.B. No. 3 the specimen was deformed continuously

to $P = 4.3$ kg and $\delta_m = 3.0$ mm without twinning. Upon reverse bending at the loading rate 0.05 cm/min, which was ten times faster than the original rate, successive twin nucleations occurred as the load increased from 2.5 to 3.5 kg. The load vs. deflection diagram of S. B. No. 3 is given in Fig. 17.

The specimen G-4 in S. B. No. 4 exhibited a marked difference in its deformation behavior compared with that of S. B. No. 3. As shown in Fig. 18, it yielded at $P \cong 2$ kg followed by a rapid work-hardening rate, and large twins were nucleated at $P = 4.8$ kg accompanied by a 47% load drop. The specimen was polished and then loaded successively to examine the growth behavior of the twins. Fig. 19 shows the thickening of the twin on the $(11\bar{2}0)$ surface of the tension side.

The center strip of this specimen G-4 was cut out into a separated specimen with a width of 3 mm by using a sectioning instrument, Semiconductor Model 716, and the new specimen was then used for S. B. No. 6. The conjugate twins were eliminated and the specimen was left with a nearly straight twin across its entire 3 mm width. The bending moment was applied about the $[11\bar{2}0]$ axis. The portion of the twin in the tension side was found to have thickened, and that in the compression side to have shrunk, as shown in Fig. 20 (a) and (b) respectively.

In S. B. No. 1 and No. 2 twins were first introduced by point loading on the (0001) surface at four different locations near the center of each specimen. The specimens were then bent in the testing machine

in such a way that the twins were on the tension side so that they would normally grow. On the contrary to the expectation the twins formed by the point loading did not grow, but new twins were nucleated at a R.S.S. of approximately 3,000 g/mm^2. Upon reverse bending, the twins formed by the simple bending were untwinned while the twins formed by the point loading remained virtually unchanged. Fig. 21 (a) clearly shows the formation of new twins crossing the original twins. Fig. 21 (b) shows the untwinning of the newly formed twins upon reverse bending.

2. Uniaxial tension tests

Table 7 lists the R.S.S. for twinning at nucleation and at growth together with other related data. The angles χ and λ between the tensile axis and respectively the twin plane and the twin direction were obtained from sterographic projection plots according to the actual orientation determined by using the back reflection Laue method. The strain rate used throughout the testing was 2.8×10^{-5} sec^{-1} which is equivalent to the crosshead speed of 0.005 cm/min averaged over the 3 cm gage length.

The specimen E-7 in the uniaxial tension test (U.T.) No. 1 was the only one not contricted. A series of parallel twins were nucleated at the C.R.S.S. τ_n = 2.85 kg/mm^2 at near the grip of the specimen. Fig. 22 (a) shows these twins on the $(11\bar{2}0)$ edge after polishing. The growth of the twins at the R.S.S. τ_g = 241 g/mm^2 is shown in Fig. 22 (b). Twin nucleation in U.T. No. 3 also occurred at the grip at τ_n = 2.24 kg/mm^2. Then, after an elongation of 4.5% a large crack was formed extending diagonally from an edge to the grip

at $\tau = 1.93$ kg/mm^2 accompanied by a load drop of 96%. The habit plane of the crack was found to be the first-order prism plane $(10\bar{1}0)$. The whole sequence of loading and unloading in U. T. No. 3 is shown in Fig. 23. The three photomicrographs in Fig. 24 show the successive stages of the thickening of a twin observed on the $(10\bar{1}0)$ surface of the specimen H-1c in U. T. No. 4. A pair of conjugate twins were nucleated at the grip at $\tau_n = 4.38$ kg/mm^2 and grew away from the grip at $\tau_g = 535$ g/mm^2. The junction of the conjugate twins is shown at the lower right-hand corner of each photomicrograph in Fig. 24. In U. T. No. 5, a twin was also nucleated at the grip but at a different stress $\tau_n = 2.32$ kg/mm^2 with a 57% load drop. Upon reloading after microscopic examination and polishing, the twin was thickened while the R.S.S. dropped from $\tau_g = 720$ g/mm^2 to 520 g/mm^2 as recorded in Fig. 25. Some unusual markings were observed on the (0001) surface inside the twin as shown in Fig. 26.

3. Point loading tests

The specimens were loaded to successively increasing load levels and examined with a microscope at each load level to determine in what load range twins were nucleated directly under the indentor. Table 8 lists the load levels at which twins were detected on the (0001) surfaces for the six indentors of varying tip radii. The average normal stresses, the load at twin nucleation divided by the indented area, are also listed in Table 8. Narrow twin lamellae were observed to grow outward from the point of application of the load in more than one of the six $<11\bar{2}0>$ directions, which were the traces of the $\{10\bar{1}2\}$

$<10\bar{1}\bar{1}>$ type twins on the (0001) surface. Fig. 27 shows such a configuration of the twin lamellae. The various specimens were loaded to different maximum loads, and the average lengths of the twin lamellae $\bar{r}$ measured from the point of application of the load to the tips of the twins were measured with a microscope. The results obtained from the testings of twenty specimens are tabulated in Table 9. A typical diagram of the load vs. the penetration of the indenter is given in Fig. 28. For the point loading experiments with the specimens 2A, 3A, and 4A the indenter having a tip radius of 0.01 mm and an apex angle of 28^{o} was used. The indentor with a tip radius of 0.015 mm and an appex angle of 27^{o} was used for the specimens 5C, 7B, 8C, and 9D. The stresses at the radial distance r and the (0001) surface were calculated by using the solutions given by Elliott (48) and by Shield (49) with some further development as described in the Appendix B. The R.S.S. acting on the twin plane in the twinning direction was calculated and listed in Table 9. The average value is 130 ± 50 g/mm^2 which can be taken as the R.S.S. required for the $\{10\bar{1}2\}<10\bar{1}\bar{1}>$ type twins to grow in the $<11\bar{2}0>$ directions.

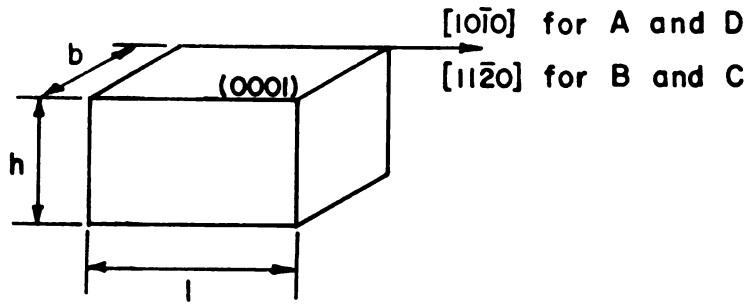

(mm)	A	B	C	D	E, F, G, & H
b	6	6	10	6	11
h	6	12	6	10	2.5
l	10	10	10	12	60

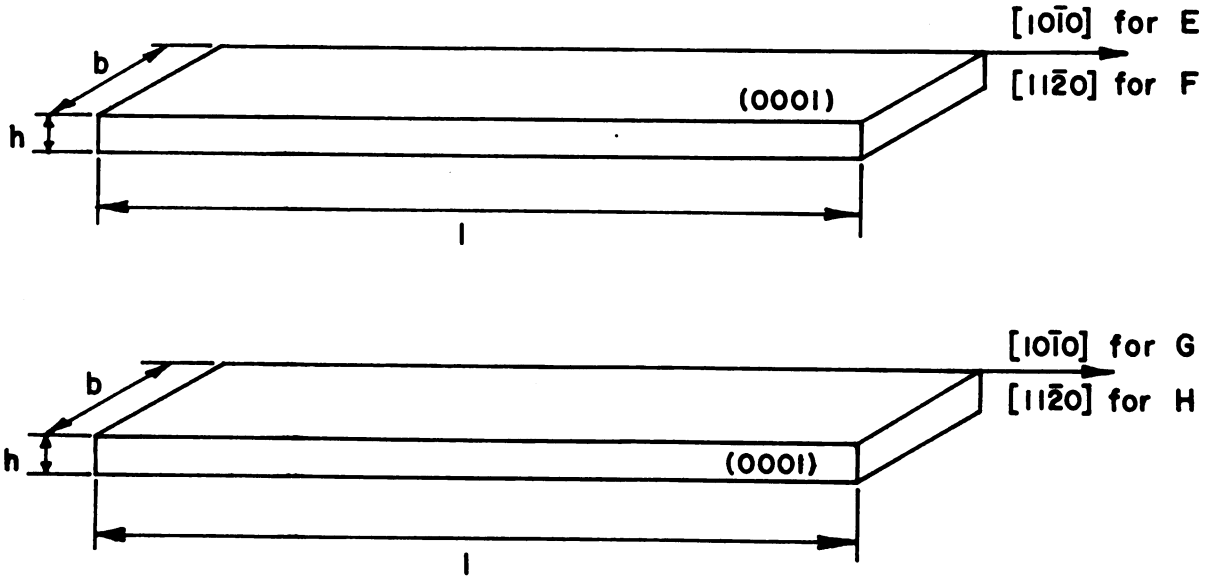

Figure 14. Orientation and dimensions of the specimens.

(a)

(b)

Figure 15. Basal slip traces across $(1\bar{1}02)[1\bar{1}0\bar{1}]$ twin boundary in S. B. No. 5. $(10\bar{1}0)$ edge of specimen F-4. 100 x. (a) P = 4.0 kg (b) P = 4.8 kg.

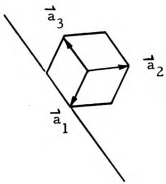

Figure 16. Twin growth in S. B. No. 5. Tension side (0001) of specimen F-4. P = 4.5 kg. 70 x.

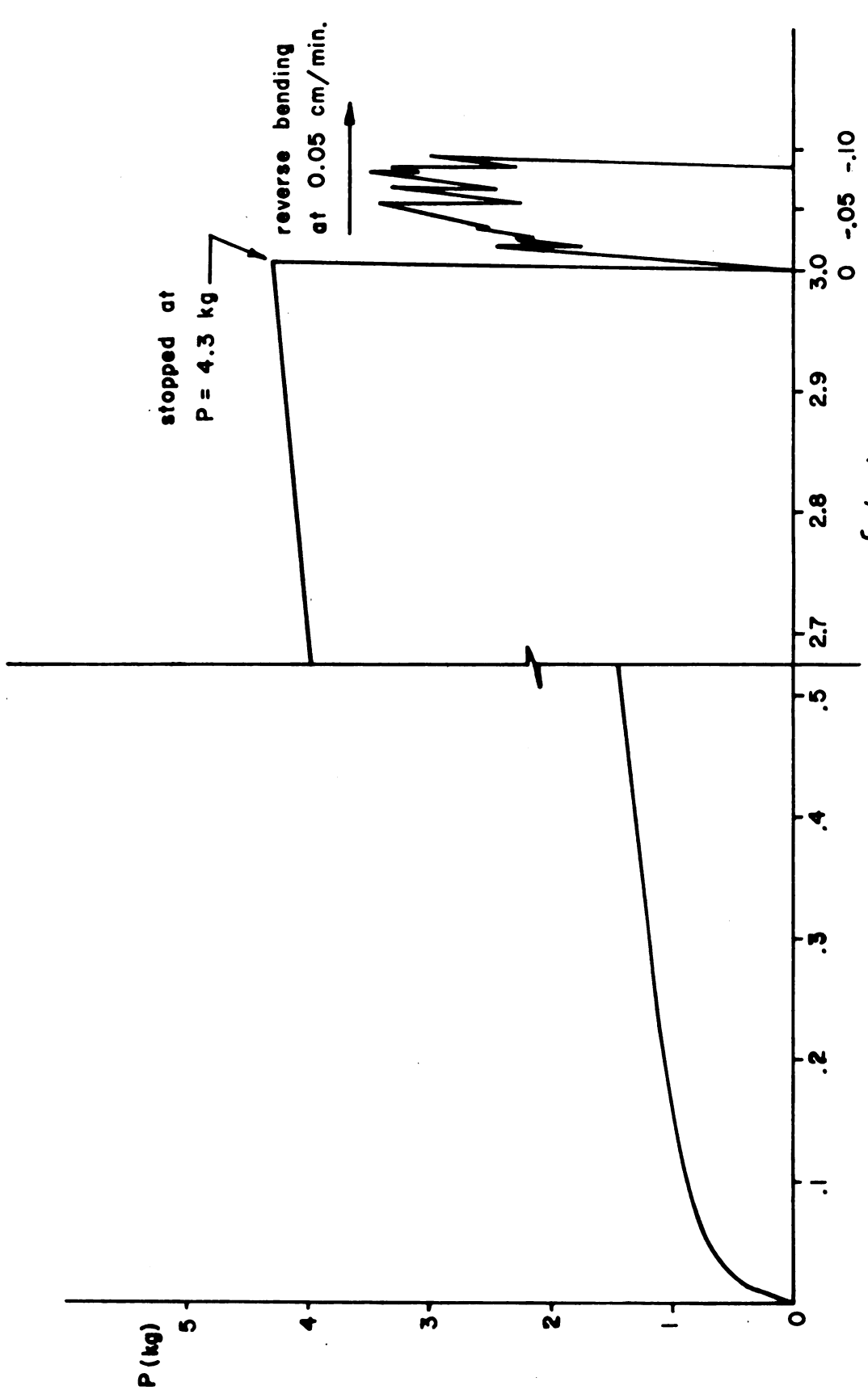

Figure 17. Load vs. deflection diagram of S. B. No. 3.
Specimen E-5. Loading rate 0.005 cm/min.

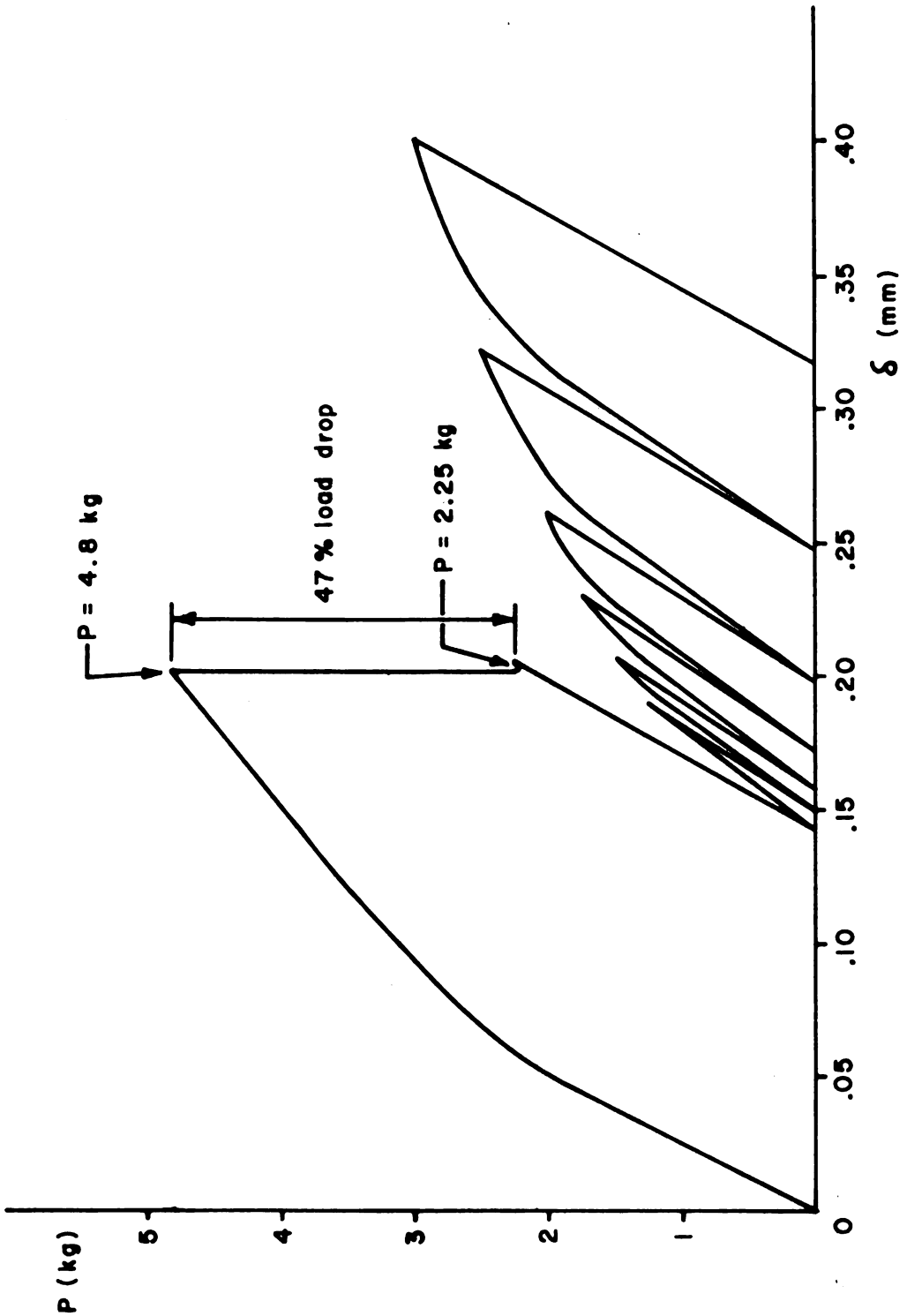

Figure 18. Load vs. deflection diagram of S. B. No. 4.
Specimen G-4. Loading rate 0.005 cm/min.

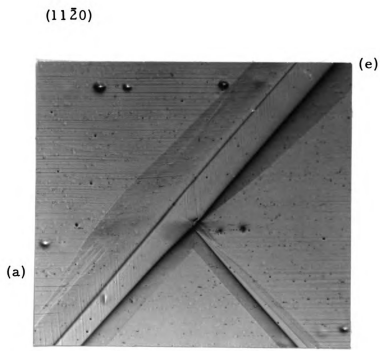

Figure 19. Growth of (1$\bar{1}$02)[1$\bar{1}$0$\bar{1}$] twin and its conjugate (1$\bar{1}$0$\bar{2}$)[$\bar{1}$10$\bar{1}$] twin in S. B. No. 4. Tension side (11$\bar{2}$0) of specimen G-4. P = 3 kg. 100x.

$(11\bar{2}0)$

(a)

$(11\bar{2}0)$

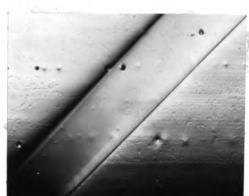

(b)

Figure 20. Growth and untwinning of $(1\bar{1}02)[1\bar{1}0\bar{1}]$ twin in S. B. No. 6. $(11\bar{2}0)$ edge of specimen G-4. P = 860 g. 70x.
(a) Growth on tension side.
(b) Untwinning on compression side.

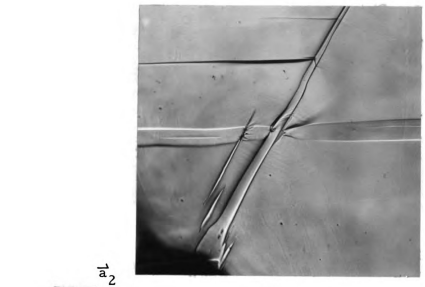

(a)

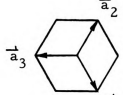

(b)

Figure 21. S. B. No. 2 after twin formation by point loading. Tension side (0001) surface of specimen E-4. 100x.
(a) Twinning.
(b) Untwinning upon reverse bending.

$(11\bar{2}0)$

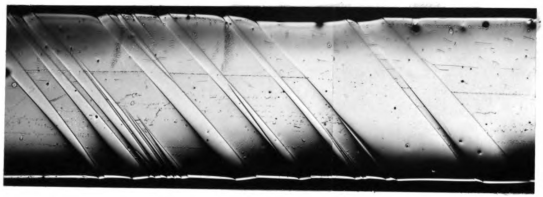

(a)

$(11\bar{2}0)$

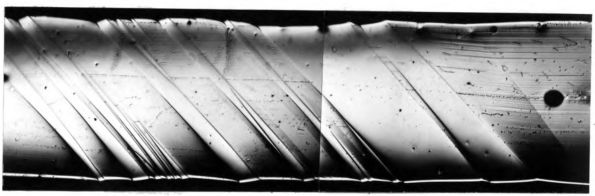

(b)

Figure 22. Twin nucleation and growth in U. T. No. 1. $(11\bar{2}0)$ edge of specimen E-7. 70 x.
(a) Nucleation of twins near at the grip after polishing. $\tau_n = 2.85$ kg/mm^2.
(b) Growth of twins. $\tau_g = 241$ g/mm^2.

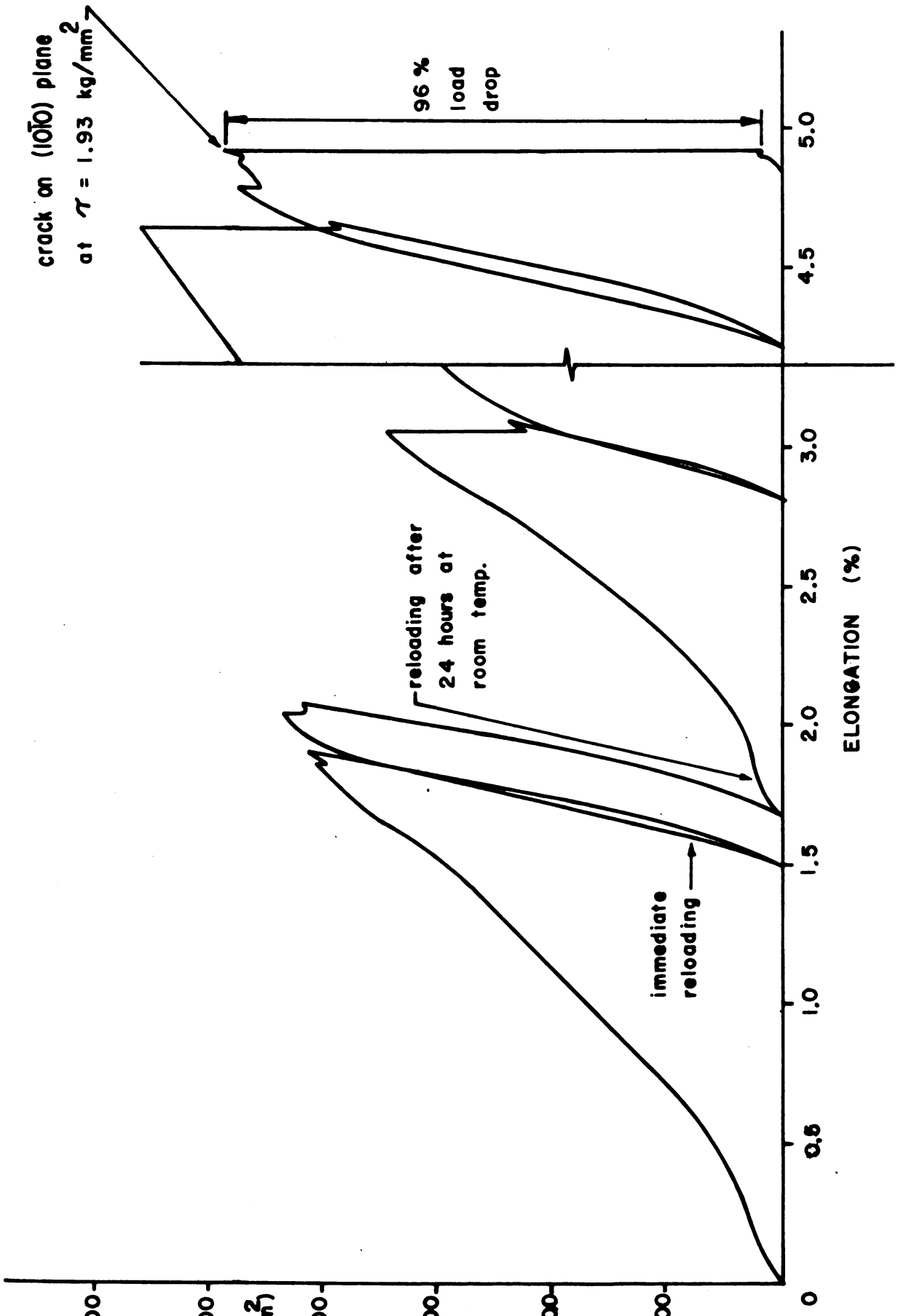

Figure 23. Stress vs. strain diagram of U. T. No. 3. Specimen F-2c. Strain rate 2.8×10^{-5} sec^{-1}.

$(10\bar{1}0)$

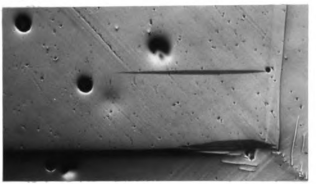

(a)

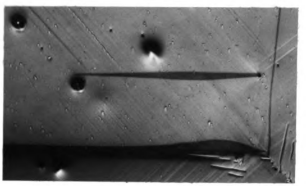

(b)

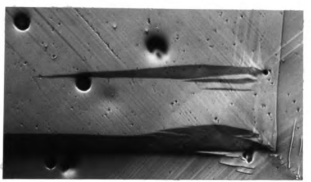

(c)

Figure 24. Twin thickening in U. T. No. 4. $(10\bar{1}0)$ surface of specimen H-1C. 120x.
(a) τ_g = 535 g/mm^2, (b) 573 g/mm^2, and
(c) 610 g/mm^2.

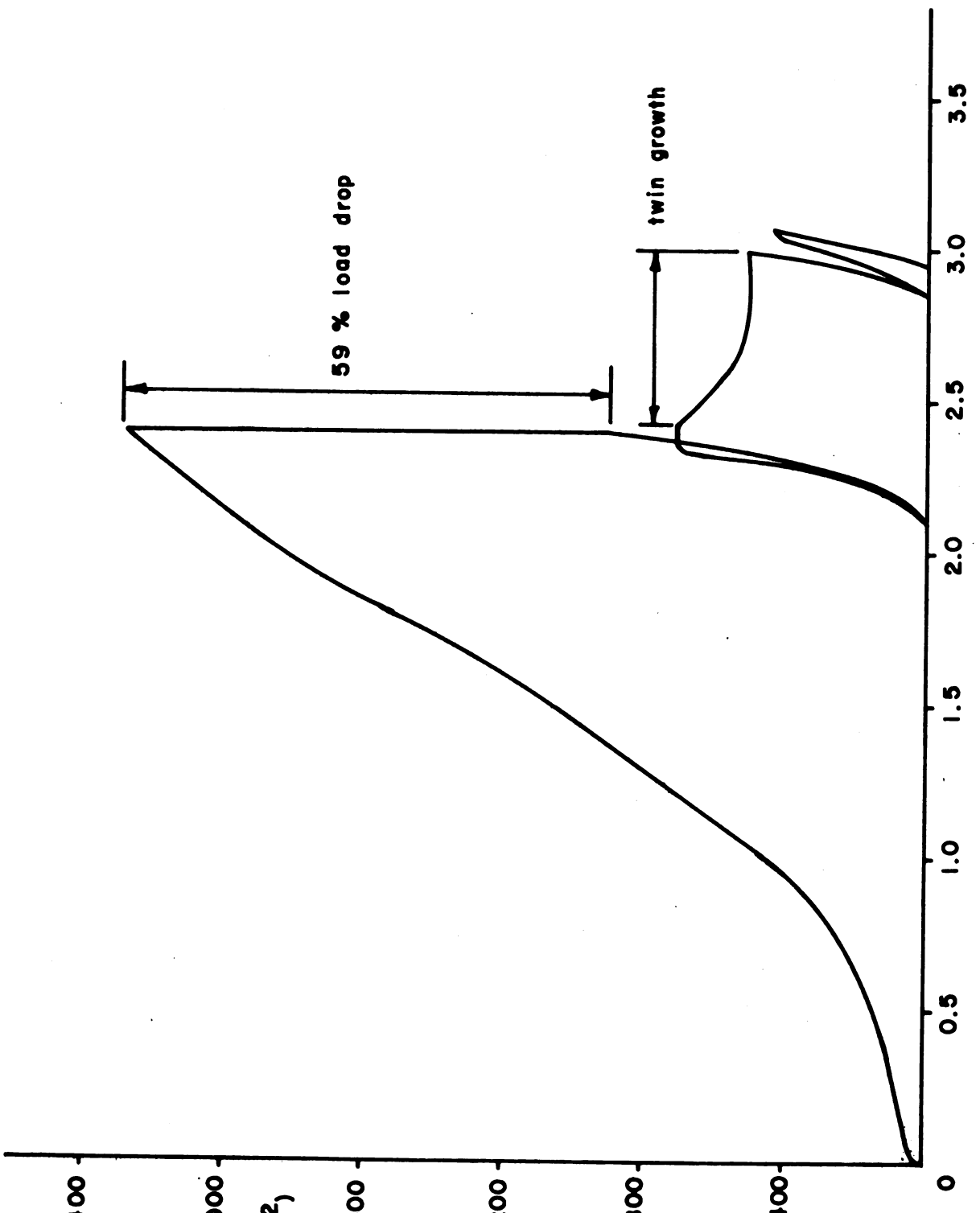

Figure 25. Stress vs. strain diagram of U. T. No. 5. Specimen F-1c. Strain rate 2.8×10^{-5} sec^{-1}.

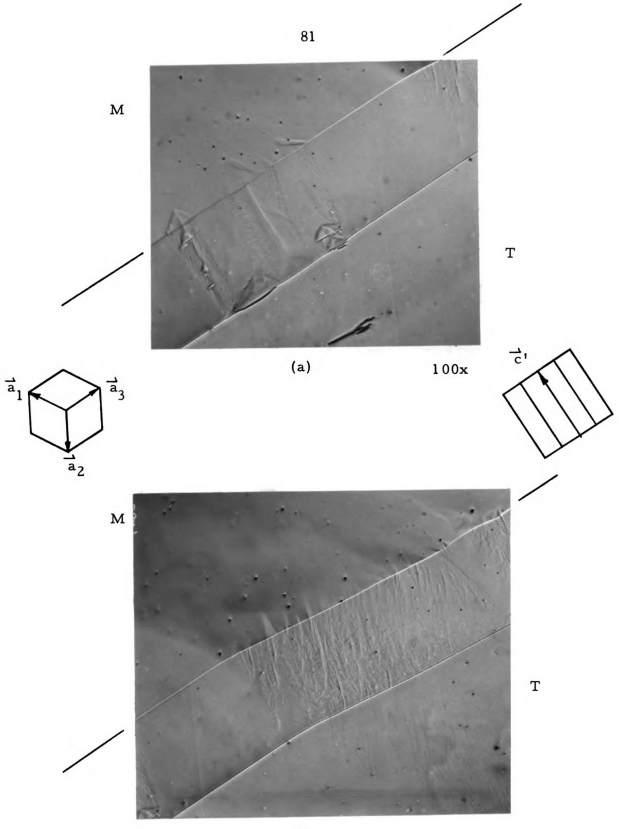

Figure 26. Twin growth in U. T. No. 5. (0001) surface of specimen F-1C. 100x.
(a) At coherent twin boundary.
(b) At incoherent twin boundary.

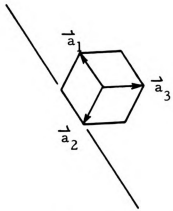

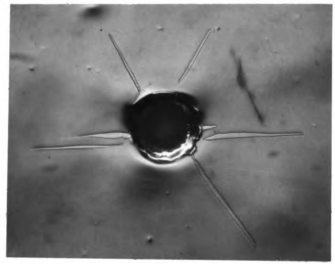

60x

Figure 27. Twin lamallae formed by the point loading to P_m = 1 kg. Specimen 2A-1 after polishing.

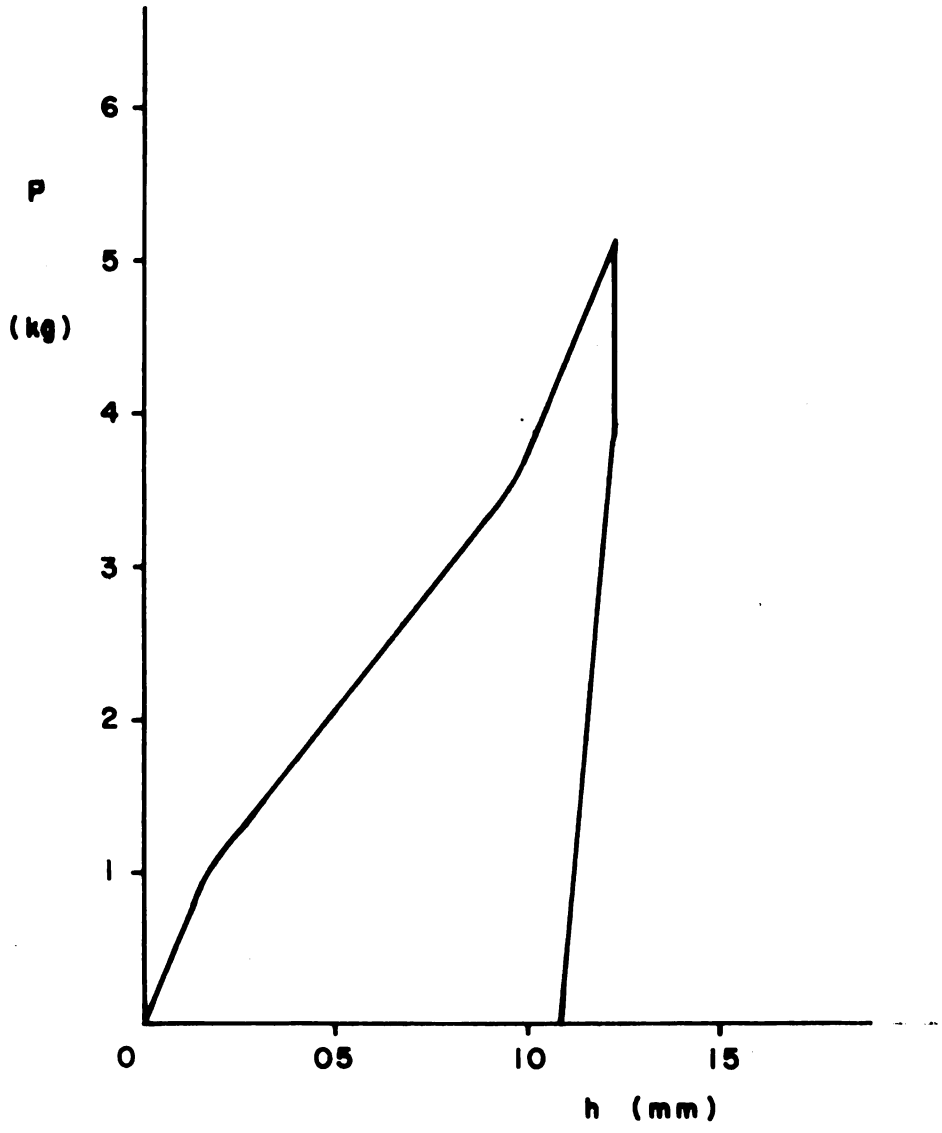

Figure 28. Load vs. penetration of the indenter diagram in point loading. Specimen 8C-3. Loading rate 0.05 cm/min.

Table 6. Simple Bending Test

No.	Orientation	Breadth b (mm)	Thickness h (mm)	Load at Twin Nucl. P_n (kg)	Max. Deflection δ_m (mm)	C.R.S.S. for Nucl. τ_n (kg)	Load at Growth P_g (kg)	R.S.S. for growth τ_g (g/mm^2)	Remarks
1	E-3	11.0	2.0	--	--	--	2.65	2,540	twin formation crossing the original twins.
2	E-4	10.5	1.5	--	--	--	2.20	3,760	the same as S.B. No. 1.
3	E-5	10.5	1.5	2.45	+ 3.0 - 0.02	4,190	--	--	twin nucleation upon reverse bending at the rate = 0.05 cm/min.
4	G-4	11.0	2.0	4.80	0.2	4,550	1.25	1,180	
5	F-4	11.0	2.0	5.55	+ 2.1 - 0.22 + 0.03	2,660	3.00	1,440	twin nucleation after a cycle of bending and reverse bending.
6	G-4	1.5	3.0	--	--	--	0.49	1,475	

Crosshead Speed = 0.005 cm/min. Beam Span L = 40 mm.

Table 7. Uniaxial Tension Test

No.	Orientation	χ (degree)	λ (degree)	$\sin\chi\cos\lambda$	Cross-Sectional Area (mm^2)	C.R.S.S. for Nucl. τ_n (kg/mm^2)	Load Relaxation (%)	Elongation at Nucl. (%)	R.S.S. for growth τ_g (g/mm^2)	Remarks
1	E-7	44	46	0.483	10	2.85	78	1.5	241	
2	G-2C*	40	40	0.492	7	3.59	75	1.7	109	
3	F-2C	45	53	0.425	11	2.24	31	4.5	--	crack on $(10\bar{1}0)$.
4	H-1C	48	52	0.458	6	4.38	72	2.5	535	
5	F-1C	40	53	0.387	11	2.32	59	2.4	720	twin growth during work-softening.

*C indicates that the specimen was constricted.
Crosshead speed = 0.005 cm/min.

Table 8. Twin Formation by Point Loading on (0001) Surface

Indentor No.	Tip Diameter (mm)	Appex Angle (degree)	Maximum Penetration h_m 10^{-2} (mm)	Diameter of Indented Area D 10^{-2} (mm)	Indented Area A 10^{-4} (mm^2)	Load at Twin Nucleation P_n (g)	Average Normal Stress $\bar{\sigma}_n$ (kg/mm^2)	Remarks
1	0.017	36	0.28	1.2	1.13	6	62.0	
7	0.07	22	0.45	3.7	10.75	18	16.75	
11	0.19	34	0.85	4.7	17.40	36	20.7	
12	0.41	19	1.40	6.0	28.30	80	28.3	
13	1.57	--	0.70	11.0	95.0	78	8.2	1/16 in. dia. steel ball.
14	2.36	--	1.10	10.5*	86.5*	78	9.0	3/32 in. dia. steel ball.

Crosshead speed = 0.005 cm/min.

* Approximate value.

Table 9. Resolved Shear Stress for Twin Growth by Point Loading on (0001) Surface

Specimen	Maximum Load P_m (kg)	Maximum Penetration h_m (mm)	Ave. Radial Length of $\bar{r}$ (mm)	Radial or Circumferencial Stress σ_{rr} or $\sigma_{\theta\theta}$ (g/mm^2)	R.S.S. for Growth τ_g (g/mm^2)
2A-1	1	0.28	0.50	296	148
2A-2	3	0.62	1.00	222	111
3A-1	1	0.25	0.55	244	122
3A-2	3	0.62	1.10	183	92
3A-3	5	0.77	1.60	189	95
4A-1	1	0.30	0.45	365	182
4A-2	1	0.30	0.45	365	182
4A-3	1	0.30	0.55	244	122
5C-1	1	0.23	0.45	365	182
5C-2	1	0.22	0.59	212	106
5C-3	3	0.67	1.10	183	92
5C-4	5	0.76	1.31	216	108
7B-1	2	0.37	0.76	256	128
7B-2	4	0.61	1.34	165	83
8C-1	1	0.24	0.60	206	103
8C-2	3	0.60	1.01	218	109
8C-3	5	0.80	1.49	166	83
9D-1	1	0.23	0.51	284	142
9D-2	3	0.50	--	--	--
9D-3	5	0.72	--	--	--

Crosshead speed = 0.05 cm/min.

V. DISCUSSION

1. Incorporation of basal slip dislocations by cross-gliding at the twin boundary

The slip traces shown in Fig. 15 (a) and (b) are continuous across the twin boundary, and their orientations are in agreement with the incorporation of $1/3[11\bar{2}0]_m$ slip dislocations in the $(1\bar{1}02)[1\bar{1}0\bar{1}]$ twin as discussed in Sec. 3.1 in Ch. II (see Fig. 8). The slip traces in the twin are distinctly sharper than those in the matrix where the sharpness of the slip band gradually diminishes at a distance away from the twin boundary. This suggests that the slip dislocations are generated in the twin and propagated under the applied stress toward the twin boundary, and then they cross-glided into the basal plane of the matrix. The slight thickening of the twin is probably due to the other incorporation process as described in Sec. 3.2, Ch. II (see Fig. 11).

2. Twin thickening by bulging out of the twin boundary in the presence of restraints

The growth process of twins through the incorporation of slip dislocations can be divided into two stages; the thickening of the existing twin by the production of twin dislocations at the twin boundary and the widening of the twin by the gliding of these twin dislocations under the applied stress. The evidences of twin thickening by the bulging out of the twin boundary as a consequence of the production of twin dislocations are given in Fig. 20 (a) and in Fig. 24 (a), (b), and (c). The basal slip traces in the matrix as well as in thickened region of the twin are in

agreement with what would be produced by the $1/3[11\bar{2}0]_m$ or $1/3[1\bar{2}10]_m$ basal slip dislocations, indicating that the incorporation processes discussed in Sec. 3.2 (see Fig. 10) and the model of twin growth developed in Sec. 4 (see Fig. 13) of Ch. II are in agreement with the experimental observations. At the later stage of deformation basal slip traces began to appear in the twin in abundance. The basal slip dislocations in the twin can also be incorporated at the twin boundary, in accordance with the same analysis described in Sec. 3.2 in Ch. II since it is entirely arbitrary to call either of the neighboring parts the twin or the matrix. The restraining effect on the bulged twin (e) in Fig. 19 appears to have been caused by the impingement of the conjugate twin under the applied stress. The free surface of the crystal was approximately 3 mm away from the site shown in Fig. 19. This seems to be also true in the specimen H-1c as shown in Fig. 24.

3. Twin growth in the absence of restraints

The growth of the twins shown in Fig. 22 (b) may be considered as having taken place in the absence of restraints. The specimen E-7 was heavily polished to an average thickness of approximately 1 mm. As shown in Fig. 22 (b) the edge of the specimen was polished down to 0.6 mm. Although there might have been thickening and widening of the twin in the growth process, only the nearly parallel growth of the original twin boundary was observed under the microscope. The R.S.S. acting on the twin dislocations was nearly the maximum for a given applied load since $\chi = \lambda = 47^\circ$. Therefore, the twin dislocations produced at the twin boundary as a result of the incorporation of basal

slip dislocations would glide to the free surfaces under the applied stress.

Fig. 16 and Fig. 27 also show the growth of twins in the absence of restraints. Fig. 16 reveals the thickening of the twin, the basal slip traces in the twin, and two sets of second-order pyramidal slip traces on the (0001) surface of the matrix. The set of traces normal to the twin boundary are the $(11\bar{2}2)[11\bar{2}\bar{3}]$ or the $(11\bar{2}\bar{2})[11\bar{2}3]$ second-order pyramidal slip traces which might have caused the twin to grow according to the incorporation process discussed in Sec. 3.3 of Ch. II (see Fig. 11). The other set might not have contributed anything to the growth of the twin since the processes described by (6), (7), (8), or (9) in Table 4 would have been involved and are very unlikely to take place. No associated traces of the second-order pyramidal slips have been detected on nonbasal planes in the present work. Further experimental investigations are necessary in order to fully understand the role the second-order pyramidal slip plays in the growth of twins. The angle between the basal slip traces in the twin and the twin boundary in Fig. 16 is an indication of the incoherency of the twin boundary and was found to be approximately 6°.

In U. T. No. 5 the stress vs. strain diagram (Fig. 27) shows a fall of the R. S. S. from 720 to 520 g/mm^2 during the twin growth. As shown in Fig. 28 some unusual surface markings triangular in shape along the coherent twin boundary and also irregular markings along the non-coherent twin boundary were observed on the (0001)

surface of the specimen F-1c. The nature of these markings and their possible relationships to the growth are not understood.

4. Twin growth and untwinning under opposite stress conditions

In S. B. No. 2 (Fig. 21) twinning by simple bending and untwinning of the twin by reverse bending were observed. Since the signs of the stresses at any point in the specimen will be reversed upon reversing the direction of the applied bending moment, the dislocation mechanism must be reversible in order to account for the twinning and untwinning in S. B. No. 2.

In S. B. No. 6 the growth of the twin on the tension side and the untwinning of the twin on the compression side were observed as shown in Fig. 20 (a) and (b). The directions of the stress components due to the applied bending moment are given in Fig. 29 (b). Since the magnitude of the normal stress was much greater than that of the shear stress, the signs of the shear stresses on the twin plane in the twinning direction are as indicated. The slip dislocations with the Burgers vector $1/3[2\bar{1}\bar{1}0]_m$ or $1/3[1\bar{2}10]_m$ on the right will move to the left toward the twin, and those with the Burgers vector $1/3[\bar{2}110]_m$ or $1/3[\bar{1}2\bar{1}0]_m$ on the left of the twin to the right. Twin dislocations will be produced at the twin boundary as shown in Fig. 29 (b) as the results of the incorporation of the slip dislocations. The notations for the twin dislocations are consistent with the sign convention described in Fig. 29 (a), where a positive twin dislocation with the Burgers vector $\vec{b}_t = e/4[1\bar{1}0\bar{1}]$ is shown. The dashed lines represent the paths of the twin dislocations under the applied shear stress acting in the neighborhood of the

corresponding twin boundaries. However, since this process may occur simultaneously at many sites along the twin boundaries, a final configuration such as shown in Fig. 20 can be resulted.

5. Resolved shear stress for twin growth

The average normal stress $\bar{\sigma}_n$ directly under the pin indenter was rather high. The R.S.S. for the twins should be approximately $1/2\ \bar{\sigma}_n$. Therefore, the apparent C.R.S.S. for the twin nucleation as a function of the size of the pin indenters varied from 4.5 to 30 kg/mm^2 as the radius of the pin indentor decreased from 1.18 to 0.009 mm. The sharp indenters actually produced the necessary stress concentration to nucleate the twins.

The average value of the R.S.S. for twin widening by point loading on (0001) surface was found to be 130 ± 50 g/mm^2. Since the twins were growing into the mechanically least disturbed regions, one might expect the resistance to the twin growth and hence the R.S.S. both to be low under such a condition. On the other hand, thickening of the twins occurred at widely scattered values of R.S.S. from 110 to 1,500 g/mm^2. It is possible that this variation in R.S.S. might have been caused by the difference in the history of plastic deformation in the various specimens, the inhomogeneous distribution of the twin lamellae, and the size and shape of the specimens.

In the simple bending and the uniaxial tension tests twin nucleations occurred at C.R.S.S. = $2.32 \sim 4.55$ kg/mm^2 accompanied always by a load drop of approximately $30 \sim 70\%$. In many cases other twins were formed which impinged on or crossed the original twins such

as shown in Fig. 19 and Fig. 21 (a) at R.S.S. = 123 ~ 3,760 g/mm^2.

Thus the R.S.S. for the twin growth by continuous thickening and widening of a twin was found to vary from 83 to 1,500 g/mm^2. This does not support a simple C.R.S.S. law for twin growth.

6. Incoherent twin boundaries and coherent twin boundary energy.

Two of the three possible shapes of twin boundaries discussed in Sec. 1.3.2 of Ch. II (see Fig. 6) have been observed; the incoherent twin boundaries shown in Fig. 19 (d) and (e) and Fig. 20 (a) and (b) are the typical examples of the type (a) in Fig. 6, whereas Fig. 19 (a) and Fig. 24 (c) show the shapes of the twin boundaries conforming to the type (c) in Fig. 6. No twin boundary of the type (b) in Fig. 6 has been observed in the present work.

In a number of cases, θ has been observed to be approximately $9^o \pm 4^o$. From Fig. 3 one finds $F_d = 2.7 \pm 0.7$ dynes/cm. Therefore, from Eq. (1-49) in Ch. II the coherent twin boundary energy is $\gamma_t = 1.4 \pm 0.4$ ergs/cm^2. The twin fault can be considered as equivalent to two coherent twin boundaries. Thus the twin fault energy is numerically equal to F_d, or 2.7 ergs/cm^2.

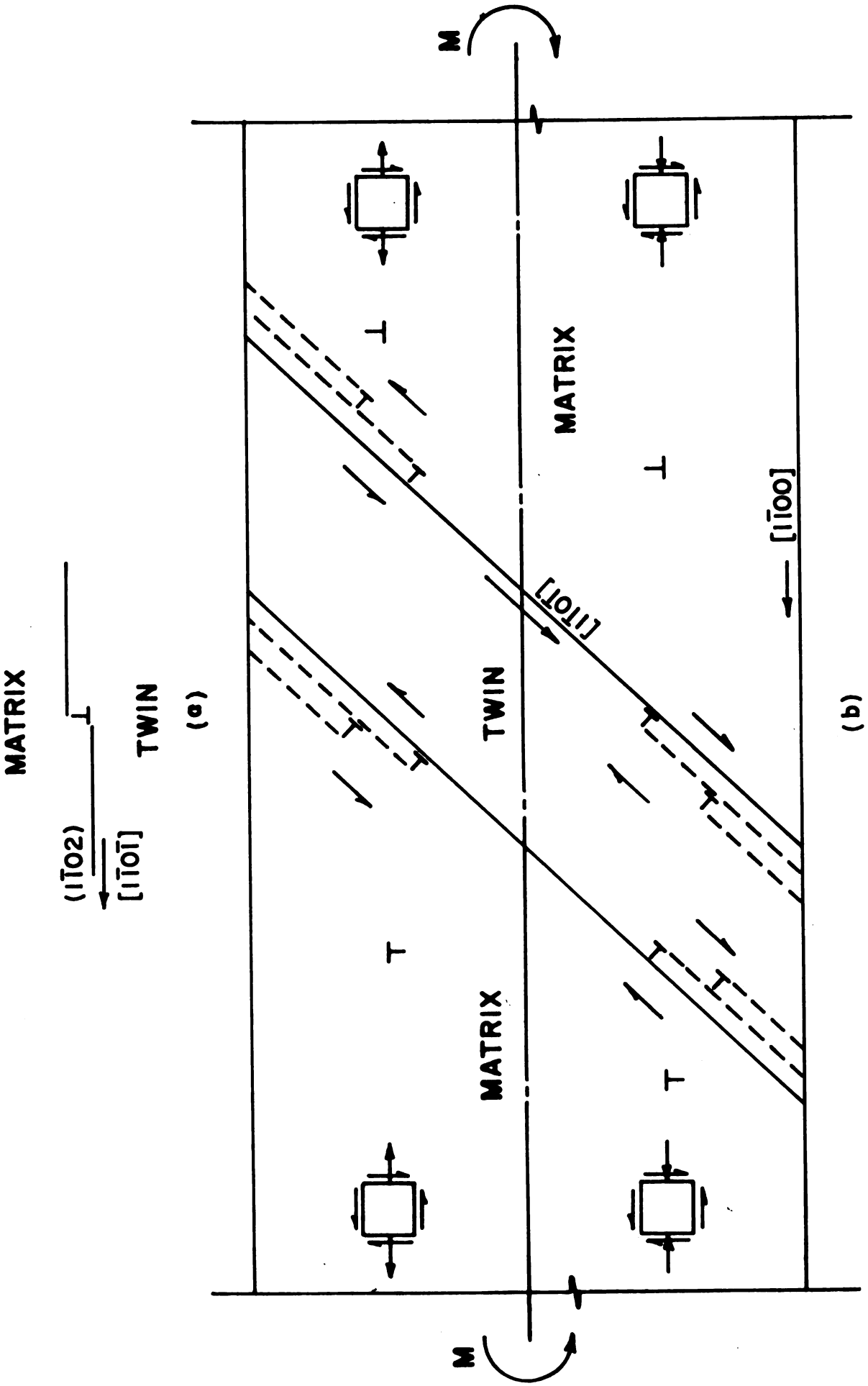

Figure 29. Twin growth and untwinning by simple bending. Plane of drawing is (11$\bar{2}$0).

VI. CONCLUSIONS

1. The incorporation of slip dislocations at the coherent twin boundary has been analyzed for the $\{1\bar{1}02\}<1\bar{1}0\bar{1}>$ type twins in hexagonal close-packed zinc crystals by applying matrix algebra and anisotropic elasticity theory of dislocations. The results indicate that a [110] screw dislocation in the matrix may cross-glide onto the basal plane in the twin with no effect on the growth or untwinning of the existing twin, whereas mixed dislocations with Burgers vectors [100] and [010] of the basal slip system and $[11\bar{1}]$ and [111] of the second-order pyramidal slip system can only be incorporated into the first-order prism planes in the twin leaving twin dislocations at the coherent twin boundary. The growth or untwinning of the existing twin depends upon whether the resolved shear stress acting on these twin dislocations is in the direction of twinning or in the opposite direction.

2. A number of zinc single crystals of various orientations were tested in simple bending, uniaxial tension, and by point loading. Experimental observations on the growth of twins support the above proposed mechanism. The resolved shear stress for the growth of twins by continuous thickening and widening of the twins was found to vary from 83 to 1,500 g/mm^2. This does not support a simple C.R.S.S. law for twin growth.

3. The interaction of a pair of twin dislocations in the edge orientation for the $\{1\bar{1}02\}<1\bar{1}0\bar{1}>$ twin system has been derived from the stress field of such a twin dislocation and found to be in general

noncentrosymmetrical. Three possible shapes of advancing twin interfaces can be predicted based on an analysis of the stable configurations of a group of twin dislocations. Two of these shapes have been observed.

4. The energy associated with the coherent boundary for the $\{1\bar{1}02\}<1\bar{1}0\bar{1}>$ twin system is estimated to be 1.4 ± 0.4 ergs/cm^2. The twin fault energy, which can be considered as twice the coherent twin boundary energy, is therefore 2.7 ± 0.8 ergs/cm^2.

5. The results of calculations of the anisotropic elastic energies of dislocations in the edge orientation also show that the following dislocation dissociation processes are energetically feasible:

$$1/3[11\bar{2}\bar{3}] \rightarrow 1/3[11\bar{2}0] + [000\bar{1}],$$
$$\Delta E = -0.25 \ln (R/r_o) \times 10^{-5} \text{ ergs/cm}$$
$$1/6[20\bar{2}\bar{3}] \rightarrow 1/3[10\bar{1}0] + 1/2[000\bar{1}],$$
$$\Delta E = -0.15 \ln (R/r_o) \times 10^{-5} \text{ ergs/cm}$$
$$1/3[11\bar{2}0] \rightarrow 1/3[10\bar{1}0] + 1/3[01\bar{1}0],$$
$$\Delta E = -1.03 \ln (R/r_o) \times 10^{-5} \text{ ergs/cm}$$
$$1/3[11\bar{2}\bar{3}] \rightarrow 1/6[20\bar{2}\bar{3}] + 1/6[02\bar{2}\bar{3}],$$
$$\Delta E = -4.21 \ln (R/r_o) \times 10^{-5} \text{ ergs/cm.}$$

APPENDIX A. Transformation of the elastic constants

The elastic stiffness constants C's and the elastic compliance constants S's relate the components of the stress and strain which are second-rank tensors.

$$\sigma_{ij} = C_{ijkl}\,\epsilon_{kl} \tag{A-1}$$

$$\epsilon_{ij} = S_{ijkl}\,\sigma_{kl} . \quad (i, j, k, l = 1, 2, \text{ or } 3) \tag{A-2}$$

They are therefore fourth-rank tensors. Upon coordinate transformation from one set of axes to another by

$$x_i' = a_{ij}\,x_j , \tag{A-3}$$

they transform in accordance with the following laws:

$$C'_{ijkl} = a_{im}\,a_{jn}\,a_{ko}\,a_{lp}\,C_{mnop} \tag{A-4}$$

$$S'_{ijkl} = a_{im}\,a_{jn}\,a_{ko}\,a_{lp}\,S_{mnop} . \tag{A-5}$$

$$(i, j, k, l, m, n, o, p = 1, 2, \text{ or } 3)$$

Each of the Eq's. (A-4) and (A-5) represents 81 equations containing 81 terms each. These 81 equations are reduced to 21 independent equations containing 21 terms each. In the case of hexagonal zinc crystal there are 5 independent elastic constants only. The generalized Hooke's law, (A-1) or (A-2), can be written in the matrix notation as follows (50):

$$\begin{pmatrix} \sigma_1 \\ \sigma_2 \\ \sigma_3 \\ \sigma_4 \\ \sigma_5 \\ \sigma_6 \end{pmatrix} = \begin{pmatrix} C_{11} & C_{12} & C_{13} & 0 & 0 & 0 \\ C_{12} & C_{11} & C_{13} & 0 & 0 & 0 \\ C_{13} & C_{13} & C_{33} & 0 & 0 & 0 \\ 0 & 0 & 0 & C_{44} & 0 & 0 \\ 0 & 0 & 0 & 0 & C_{44} & 0 \\ 0 & 0 & 0 & 0 & 0 & 1/2(C_{11}-C_{12}) \end{pmatrix} \begin{pmatrix} \epsilon_1 \\ \epsilon_2 \\ \epsilon_3 \\ \epsilon_4 \\ \epsilon_5 \\ \epsilon_6 \end{pmatrix} \qquad \text{(A-6)}$$

$$\begin{pmatrix} \epsilon_1 \\ \epsilon_2 \\ \epsilon_3 \\ \epsilon_4 \\ \epsilon_5 \\ \epsilon_6 \end{pmatrix} = \begin{pmatrix} S_{11} & S_{12} & S_{13} & 0 & 0 & 0 \\ S_{12} & S_{11} & S_{13} & 0 & 0 & 0 \\ S_{13} & S_{13} & S_{33} & 0 & 0 & 0 \\ 0 & 0 & 0 & S_{44} & 0 & 0 \\ 0 & 0 & 0 & 0 & S_{44} & 0 \\ 0 & 0 & 0 & 0 & 0 & 2(S_{11} - S_{12}) \end{pmatrix} \begin{pmatrix} \sigma_1 \\ \sigma_2 \\ \sigma_3 \\ \sigma_4 \\ \sigma_5 \\ \sigma_6 \end{pmatrix} \qquad \text{(A-7)}$$

or

$$\sigma_r = C_{rs}\, \epsilon_s$$

$$\epsilon_r = S_{rs}\, \sigma_s \quad . \qquad (r, s = 1, 2, \ldots\ldots, 6)$$

The stress components and the strain components are written with a single suffix from 1 to 6.

$$\begin{pmatrix} \sigma_{11} & \sigma_{12} & \sigma_{31} \\ \sigma_{12} & \sigma_{22} & \sigma_{23} \\ \sigma_{31} & \sigma_{23} & \sigma_{33} \end{pmatrix} \longrightarrow \begin{pmatrix} \sigma_1 & \sigma_6 & \sigma_5 \\ \sigma_6 & \sigma_2 & \sigma_4 \\ \sigma_5 & \sigma_4 & \sigma_3 \end{pmatrix} ,$$

$$\begin{pmatrix} \epsilon_{11} & \epsilon_{12} & \epsilon_{31} \\ \epsilon_{12} & \epsilon_{22} & \epsilon_{23} \\ \epsilon_{31} & \epsilon_{23} & \epsilon_{33} \end{pmatrix} \rightarrow \begin{pmatrix} \epsilon_1 & 1/2\,\epsilon_6 & 1/2\,\epsilon_5 \\ 1/2\,\epsilon_6 & \epsilon_2 & 1/2\,\epsilon_4 \\ 1/2\,\epsilon_5 & 1/2\,\epsilon_4 & \epsilon_3 \end{pmatrix} .$$

In the S_{ijkl} and C_{ijkl} the first two suffices are abbreviated into a single one running from 1 to 6, and the last two are abbreviated in the same way, according to the following scheme:

tensor notation	11	22	33	23, 32	31, 13	12, 21
matrix notation	1	2	3	4	5	6

At the same time factors of 2 and 4 are introduced as follows:

$S_{ijkl} = S_{rs}$ when r and s are 1, 2, or 3

$2S_{ijkl} = S_{rs}$ when either r or s are 4, 5, or 6

$4S_{ijkl} = S_{rs}$ when both r and s are 4, 5, or 6

To transform the elastic constants upon coordinate transformation it is necessary to go back to the tensor notation. The composite equations (A-4) and (A-5) can be simplified considerably when the transformation is a rotation of the axes about one of the axes (28).

APPENDIX B. Calculation of the resolved shear stress for twin growth in the point loading experiments

(a) Fundamental formulae

Three-dimensional stress distributions in hexagonal aeolotropic materials were analyzed by Elliott (48), who obtained a general solution of the elastic equations of equilibrium in terms of two harmonic functions. He also showed that in the case of axially symmetrical stress system the solutions might be written in terms of a single stress function. The following is a brief account of Elliott's solution.

If one chooses coordinate axes so that the axes x_1 and x_2 are parallel to the basal plane and the x_3 axis normal to the basal plane, the equation (A-6) or (A-7) describes precisely the stress-strain relationship.

Neglecting the body forces the equation of equilibrium are

$$\frac{\partial \sigma_{ij}}{\partial x_j} = 0 \quad . \qquad (i, j = 1, 2, \text{ or } 3) \tag{B-1}$$

Also, if u_1, u_2, and u_3 are the displacements, then

$$\epsilon_{ij} = \frac{1}{2}\left(\frac{\partial u_i}{\partial x_j} + \frac{\partial u_j}{\partial x_i}\right) \qquad \text{when } i = j$$

and (B-2)

$$\gamma_{ij} = 2\epsilon_{ij} = \frac{\partial u_i}{\partial x_j} + \frac{\partial u_j}{\partial x_i} \qquad \text{when } i \neq j \, .$$

One can obtain the equations of equilibrium in terms of the displacements by substituting (B-2) into (A-6) and into (B-1).

Assume a solution such that

$$u_1 = \frac{\partial \phi}{\partial x_1} , \quad u_2 = \frac{\partial \phi}{\partial x_2} , \quad u_3 = \frac{\partial \phi}{\partial x_3} , \tag{B-3}$$

where $\phi = \phi(x_1, x_2, x_3)$ is a strain potential function. Substituting the relationships (B-3) into the equations of equilibrium expressed in terms of the displacements, one will arrive at the characteristic equation

$$C_{11}C_{44}\nu^2 + [\, C_{13}(2C_{44}+C_{13}) - C_{11}C_{33}]\, \nu + C_{33}C_{44} = 0 \tag{B-4}$$

or

$$(S_{13}^2 - S_{11}S_{33})\nu^2 - [\, 2S_{13}(S_{12}-S_{11}) - S_{11}S_{44}]\, \nu + S_{12}^2 - S_{11}^2 = 0 , \tag{B-5}$$

which is a quadradic equation in ν with roots ν_1 and ν_2. The roots ν_1, ν_2 may be real or complex depending upon the elastic constants; they are real, for example, in the case of magnesium but are complex conjugates for zinc. The corresponding values of k's are

$$k_i = \frac{\nu_i C_{11} - C_{44}}{C_{13} + C_{44}} . \quad (i = 1, 2) \tag{B-6}$$

The possible functions ϕ's are the solutions of

$$(\nabla_1^2 + \nu_i \frac{\partial^2}{\partial x_3^2})\, \phi_i = 0 \qquad (i = 1, 2) \tag{B-7}$$

where

$$\nabla_1^2 = \frac{\partial^2}{\partial x_1^2} + \frac{\partial^2}{\partial x_2^2} \tag{B-8}$$

also

$$u_1 = \frac{\partial \phi_1}{\partial x_1} + \frac{\partial \phi_2}{\partial x_1}$$

$$u_2 = \frac{\partial \phi_1}{\partial x_2} + \frac{\partial \phi_2}{\partial x_2} \qquad \text{(B-9)}$$

$$u_3 = k_1 \frac{\partial \phi_1}{\partial x_3} + k_2 \frac{\partial \phi_2}{\partial x_3} \quad .$$

Since the material is transversely symmetric, for an axially symmetric stress distribution the solutions are better expressed in the cylindrical coordinate system (r, θ, z). The governing equations become

$$(\nabla_1^2 + \nu_i \frac{\partial^2}{\partial z^2}) \phi_i = 0 \qquad (i = 1, 2) \qquad \text{(B-10)}$$

where

$$u_r = \frac{\partial}{\partial r} (\phi_1 + \phi_2) \qquad \text{(B-11)}$$

and also

$$w = k_1 \frac{\partial \phi_1}{\partial z} + k_2 \frac{\partial \phi_2}{\partial z} \quad . \qquad \text{(B-12)}$$

The stress components are given by

$$\sigma_{rr} = [C_{11} \frac{\partial^2}{\partial r^2} + C_{12} (\frac{1}{r} \frac{\partial}{\partial r} + \frac{1}{r^2} \frac{\partial^2}{\partial \theta^2})] (\phi_1 + \phi_2)$$

$$+ C_{33} (k_1 \frac{\partial^2 \phi_1}{\partial z^2} + k_2 \frac{\partial^2 \phi_2}{\partial z^2})$$

$$\sigma_{\theta\theta} = [C_{12} \frac{\partial^2}{\partial r^2} + C_{11} (\frac{1}{r} \frac{\partial}{\partial r} + \frac{1}{r^2} \frac{\partial^2}{\partial \theta^2})] (\phi_1 + \phi_2)$$

$$+ C_{13} (k_1 \frac{\partial^2 \phi_1}{\partial z^2} + k_2 \frac{\partial^2 \phi_2}{\partial z^2})$$

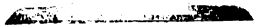

$$\sigma_{zz} = (k_1 C_{33} - \nu_1 C_{13}) \frac{\partial^2 \phi_1}{\partial z^2} + (k_2 C_{33} - \nu_2 C_{13}) \frac{\partial^2 \phi_2}{\partial z^2}$$

$$\sigma_{r\theta} = (C_{11} - C_{12})\left[\frac{1}{r} \frac{\partial^2}{\partial r \partial \theta} - \frac{1}{r^2} \frac{\partial}{\partial \theta}\right] (\phi_1 + \phi_2) \qquad \text{(B-13)}$$

$$\sigma_{\theta z} = C_{44}\left[(1 + k_1) \frac{1}{r} \frac{\partial^2 \phi_1}{\partial \theta \partial z} + (1 + k_2) \frac{1}{r} \frac{\partial^2 \phi_2}{\partial \theta \partial z}\right]$$

$$\sigma_{rz} = C_{44}\left[(1 + k_1) \frac{1}{r} \frac{\partial^2 \phi_1}{\partial r \partial z} + (1 + k_2) \frac{1}{r} \frac{\partial^2 \phi_2}{\partial r \partial z}\right]$$

Because of the axial symmetry $\sigma_{r\theta} = \sigma_{\theta z} = 0$.

The three-dimensional stress distributions at any point in the medium can be determined when the proper functions ϕ_1 and ϕ_2 for a given problem are judiciously chosen and the arbitrary constants in these functions are determined by satisfying the boundary conditions.

(b) The solutions

The specimens will be considered as a semi-infinite medium acted upon by a concentrated force P in the -z direction. Shield (49) introduced the following potential functions for such a problem:

$$\phi_1 = \frac{F}{8\pi(\nu_1 - \nu_2)} \log \frac{R_1 + Z_1}{R_1 - Z_1}$$

$$\phi_2 = -\frac{F}{8\pi(\nu_1 - \nu_2)} \log \frac{R_2 + Z_2}{R_2 - Z_2} \qquad \text{(B-14)}$$

where $F = P \frac{(C_{13} + C_{44})}{C_{11} C_{44}}$, $R_i^2 = r^2 + z_i^2$, $z_i = \nu_i^{-1/2} z$ (B-15)

In applying these general solutions (B-14) to the problem on hand to calculate the stresses at $z = 0$ plane, an approximation is

made that the depth of penetration of the indentor is neglected due to its smallness in comparison with the distance from the origin to the point of interest on the $z = 0$ surface. The following results are obtained for $z = 0$:

$$u_r = \frac{F}{2\pi\beta(\nu_1 - \nu_2)} \left(\frac{\sqrt{\nu_1}}{1+k_1} - \frac{\sqrt{\nu_2}}{1+k_2}\right) \left\{\frac{k_1 C_{33} - \nu_1 C_{13}}{\nu_1} - \frac{k_2 C_{33} - \nu_2 C_{13}}{\nu_2}\right\} \frac{1}{r} \tag{B-16}$$

$$w = \frac{Fa}{2\pi\beta(\nu_1 - \nu_2)} \left\{\frac{k_1 C_{33} - \nu_1 C_{13}}{\nu_1} - \frac{k_2 C_{33} - \nu_2 C_{13}}{\nu_2}\right\} \frac{1}{r} \tag{B-17}$$

where

$$a = \frac{k_1}{1+k_1} - \frac{k_2}{1+k_2} \tag{B-18}$$

$$\beta = \frac{k_1 C_{33} - \nu_1 C_{13}}{\sqrt{\nu_1(1+k_1)}} - \frac{k_2 C_{33} - \nu_2 C_{13}}{\sqrt{\nu_2(1+k_2)}} \tag{B-19}$$

and

$$\sigma_{rr} + \sigma_{\theta\theta} = (C_{11} + C_{12} - \frac{2C_{13}^2}{C_{33}}) \left(\frac{\partial u_r}{\partial r} + \frac{u_r}{r}\right) \tag{B-20}$$

$$\sigma_{rr} - \sigma_{\theta\theta} = (C_{11} - C_{12}) \left(\frac{\partial u_r}{\partial r} - \frac{u_r}{r}\right) . \tag{B-21}$$

The roots of the characteristic equation (B-4) or (B-5) for zinc crystals are found to be

$$\nu_i = 0.2819 + 0.5476\, j \qquad (i = 1, 2) \tag{B-22}$$

using the elastic constants in Table 1. Let

$$A = -\frac{P(C_{13} + C_{44})}{2\pi\beta(\nu_1 - \nu_2)C_{11}C_{44}} \left(\frac{\sqrt{\nu_1}}{1+k_1} - \frac{\sqrt{\nu_2}}{1+k_2}\right) \left\{\frac{k_1 C_{33} - \nu_1 C_{13}}{\nu_1} - \frac{k_2 C_{33} - \nu_2 C_{13}}{\nu_2}\right\} \tag{B-23}$$

then after proper substitutions the numerical value of A is

$$A = P \times 5.84 \times 10^{-14} \quad . \tag{B-24}$$

Thus

$$\frac{u_r}{r} = -\frac{A}{r^2} \tag{B-25}$$

$$\frac{\partial u_r}{\partial r} = \frac{A}{r^2} \tag{B-26}$$

Combining (B-20) and (B-21) and substituting (B-25) and (B-26) the nonvanishing stress components at $z = 0$ are

$$\sigma_{rr} = (C_{11} - C_{12}) \frac{A}{r^2} \tag{B-27}$$

$$\sigma_{\theta\theta} = (C_{12} - C_{11}) \frac{A}{r^2} \tag{B-28}$$

Hence

$$\frac{\sigma_{rr}}{P} = -\frac{\sigma_{\theta\theta}}{P} = \frac{74}{r^2} \times 10^{-3} \tag{B-29}$$

A plot of $\frac{\sigma_{rr}}{P}$ and $-\frac{\sigma_{\theta\theta}}{P}$ vs. r is shown in Fig. 30. The shear stress, τ, on the $\{10\bar{1}2\}$ plane in the $<10\bar{1}\bar{1}>$ directions is obtained by a transformation

$$\sigma'_{ij} = a_{ik} a_{jl} \sigma_{kl} \quad , \tag{B-30}$$

where

$$a_{ij} = \begin{pmatrix} \cos\phi & \sin\phi \\ -\sin\phi & \cos\phi \end{pmatrix} \quad . \tag{B-31}$$

Thus $\tau = \sigma'_{12} = \sin\phi \cos\phi \, \sigma_{11}$.

Since $\phi = 47^{o}$ and $\sigma_{11} = \sigma_{\theta\theta}$,

$$\tau = \frac{1}{2} \sigma_{\theta\theta} \quad . \tag{B-32}$$

It is of interest to compare the Eq. (B-29) with that calculated by assuming the crystal to be isotropic. Using the solutions by Sneddon et al (51), Young's and shear moduli for zinc given in Table 1, and a Poisson's ratio of 1/3, the results are

$$\frac{\sigma_{rr}}{P} = - \frac{\sigma_{\theta\theta}}{P} = \frac{110}{r^2} \times 10^{-3} \quad . \tag{B-33}$$

This is 50% higher than that given in Eq. (B-29) as far as the stresses in the $z = 0$ plane are concerned. It seems apparent that crystal anisotropy should be taken into consideration for this kind of problems.

APPENDIX C. Calculation of the resolved shear stress for twin growth by simple bending

The stress vs. strain diagram is simplified to that shown in Fig. 31 (a) and is assumed to be the same in tension and compression. The flexure stress distribution shown in Fig. 31 (b) can be applied after a large amount of deformation well beyond the elastic limit has taken place. In computing the stresses in terms of the applied moment the stresses corresponding to the triangular areas abc and bde in Fig. 31 (b) may be neglected without unduly impairing the accuracy. They contribute little resistance to the applied bending moment M, owing to their short moment arms. Hence the simplification of the stress distribution to that shown in Fig. 31 (c) is permissible.

The whole upper half of the beam is subjected to a uniform compressive stress $-\sigma$, while the lower half is under a uniform tension $+\sigma$. Therefore, an equilibrium equation can be obtained as

$$M = \sigma \left(\frac{bh}{2}\right) \left(\frac{h}{2}\right) = \frac{1}{4} \sigma b h^2 . \qquad (C-1)$$

The maximum flexure stress σ_m is at the center of the beam span L where the bending moment is also the maximum; $M_m = \frac{1}{2} PL$. Thus,

$$\sigma_m = 2 \frac{PL}{bh^2} . \qquad (C-2)$$

The distribution of the shear stress is simplified as shown in Fig. 31 (d). The magnitude of the shear stress becomes

$$\tau = \frac{1}{2} \frac{P}{bh} . \qquad (C-3)$$

The resolved shear stress for the twin τ_t is obtained from the transformation equations (B-30) and (B-31).

$$\tau_t = \sin \phi \cos \phi \, \sigma_m + \cos^2 \phi \, \tau$$

where $\phi = 47^o$. Hence

$$\tau_t = \frac{PL}{bh^2} + 0.233 \frac{P}{bh} . \qquad (C-4)$$

In the above development, the material is considered to be "perfectly plastic" at the stage of twin formation. This assumption is justified for the simple bending tests, since the load vs. deformation curves recorded such as shown in Fig. 17 can be closely approximated to the elastic-perfectly plastic stress vs. strain diagram given in Fig. 31 (a).

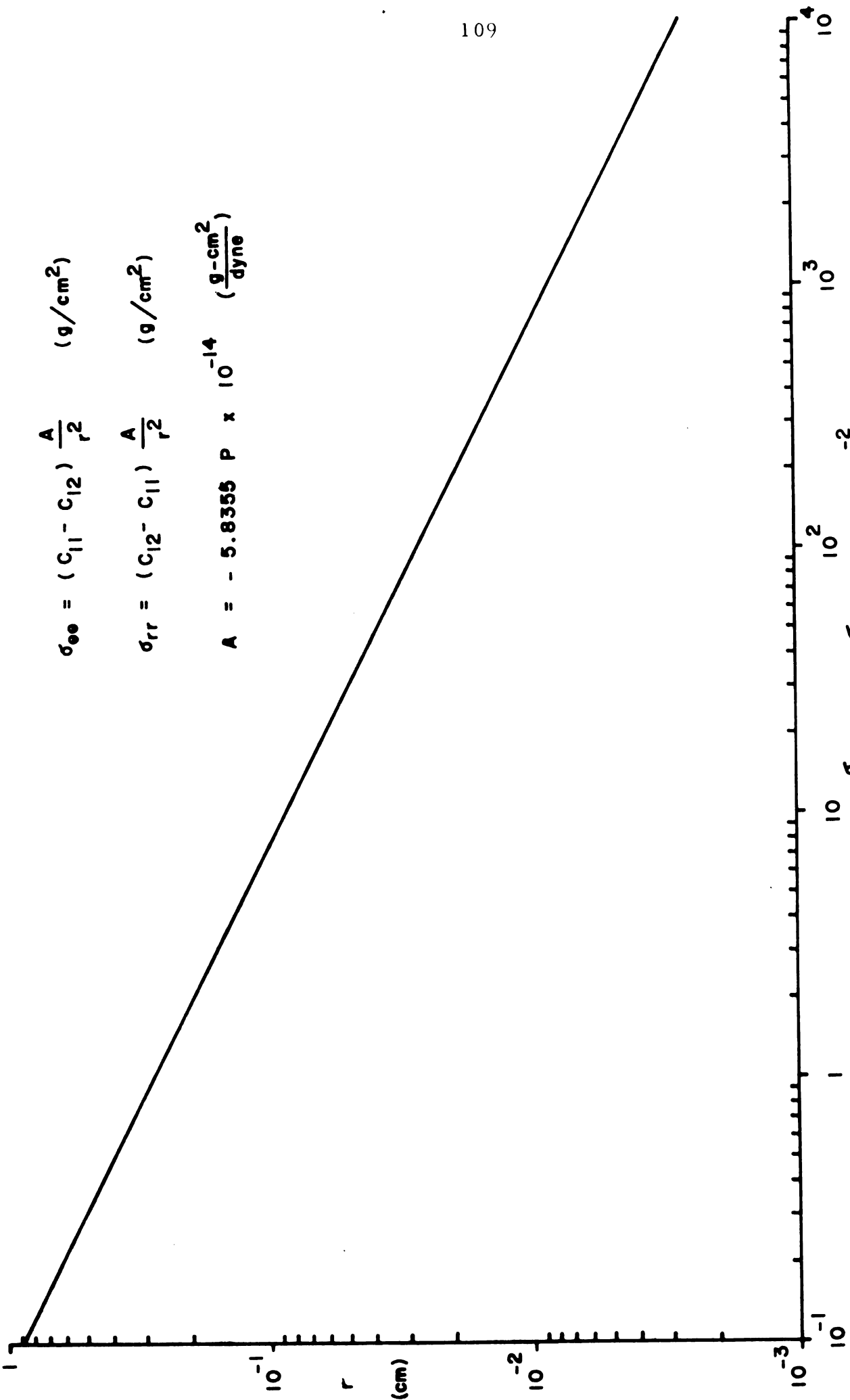

Figure 30. Radial and circumferential stress vs. radial distance at (0001) surface by point loading.

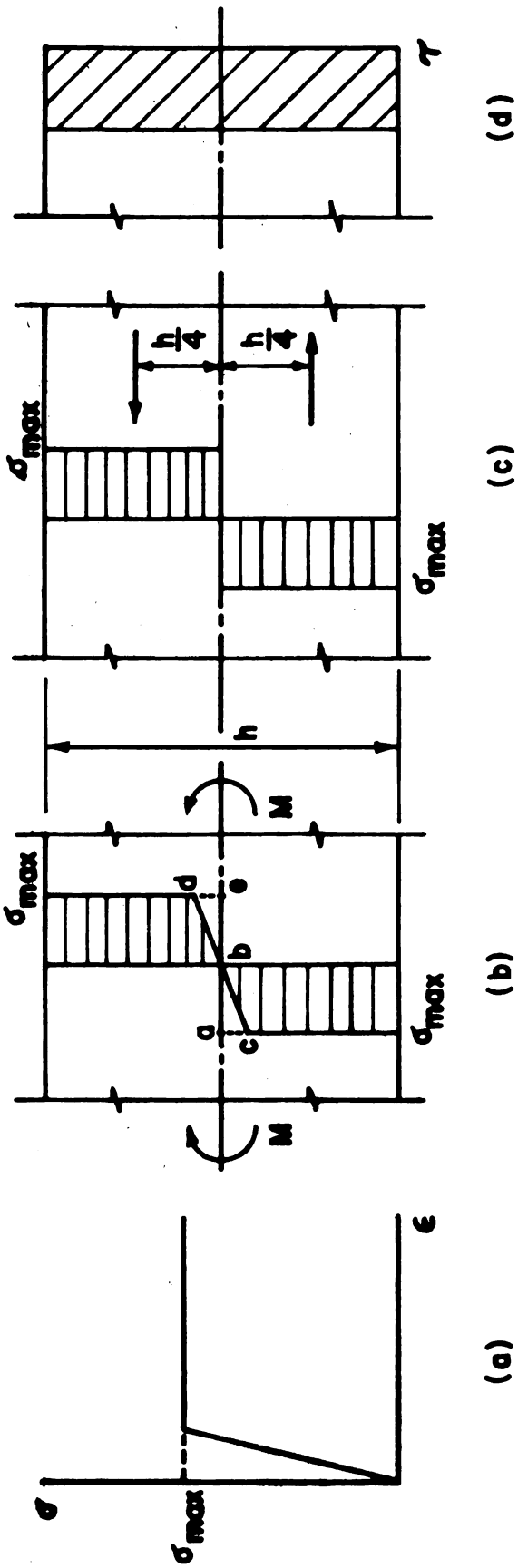

Figure 31. Stress distribution by simple bending.

BIBLIOGRAPHY

1. Barrett, C. S., Structure of Metals, p. 376, McGraw Hill Inc., New York (1952).
2. Cahn, R. W., Adv. in Phys., 3, 363 (1954).
3. Jawson, M. A. and Dove, D. B., Acta Cryst., 13, 232 (1960).
4. Kiho, H., J. Phys. Soc. Japan, 9, 739 (1954).
5. Mathewson, C. H., Trans. A. I. M. E., 76, 554 (1928).
6. Barrett, C. S., Cold Working of Metals, p. 78, A. S. M., Cleveland (1949).
7. Cottrell, A. H., Dislocation and Plastic Flow in Crystals, p. 9, Oxford Univ. Press, London (1953).
8. Cottrell, A. H. and Bilby, B. A., Phil. Mag., Ser. 7, 42, 573 (1951).
9. Thompson, N. and Millard, D. J., Phil. Mag., Ser. 7, 43, 422 (1952).
10. Sleeswyk, A. W. and Verbraak, C. A., Acta Met., 9, 917 (1961).
11. Sleeswyk, A. W., Acta Met., 10, 705 (1962).
12. Votava, E. and Sleeswyk, A. W., Acta Met., 10, 965 (1962).
13. Ogawa, K. and Maddin, R., Acta Met., 12, 713 (1964).
14. Ishii, K. and Kiho, H., J. Phys. Soc. Japan, 18, 1122 (1963).
15. Ishii, K. and Kiho, H., J. Phys. Soc. Japan, 18, 1133 (1963).
16. Fourie, J. T., Weinberg, F., and Boswell, F. W. C., Acta Met. 8, 851 (1960).
17. Blewitt, T. H., Coltman, R. R., and Redman, J. K., J. Appl. Phys., 28, 651 (1957).

18. Suzuki, H. and Barrett, C. S., Acta Met., 6, 156 (1958).

19. Venables, J. A., Phil. Mag., 6, 379 (1961).

20. Cohen, J. B. and Weertman, J., Acta Met., 11, 997 (1963).

21. Venables, J. A., J. Phys. Chem. Solids, 25, 685 (1964).

22. Venables, J. A., J. Phys. Chem. Solids, 25, 693 (1964).

23. Orowan, E., Dislocations in Metals, A. I. M. E., New York, p. 116 (1954).

24. Bell, R. L. and Cahn, R. W., Proc. Roy. Soc. (London), A239, 494 (1957).

25. Price, P. B., Proc. Roy. Soc. (London), A260, 251 (1961).

26. Taylor, A. and Kagle, B. J., Crystallographic Data on Metal and Alloy Structures, p. 263, Dover, New York (1962).

27. Huntington, H. B., Solid State Physics, p. 213, Academic Press Inc., New York (1958).

28. Hearmon, R. F. S., An Introduction to Applied Anisotropic Elasticity, p. 44, Oxford Univ. Press, London (1961).

29. Burgers, J. M., Proc. Acad. Sci. Amst., 42, 378 (1939).

30. Eshelby, J. D., Phil. Mag., 40, 903 (1949).

31. Leibfreid, G., Z. für Physik, 135, 23 (1953).

32. Eshelby, J. D., Read, W. T., and Shockley, W., Acta Met., 1, 251 (1953).

33. Seeger, A. and Schöck, G., Acta Met., 1, 519 (1953).

34. Foreman, A. J. E., Acta Met., 3, 322 (1955).

35. Chou, Y. T. and Eshelby, J. D., J. Mech. Phys. Solids, 10, 27 (1962).

36. Chou, Y. T., Acta Met., 10, 739 (1962).

37. Chou, Y. T., J. Appl. Phys., 33, 2747 (1962).

38. Cottrell, A. H., Dislocation and Plastic Flow in Crystals, p. 46, Oxford Univ. Press, London (1953).

39. Frank, F. C., Phil. Mag., 42, 809 (1951).

40. Frank, F. C. and Nicholas, J. F., Phil. Mag., 44, 1213 (1953).

41. Price, P. B., Electron Microscopy and Strength of Crystals, p. 41, Interscience Publ., New York (1963).

42. Hohn, F. E., Elementary Matrix Algebra, p. 179, Macmillan Co., New York (1958).

43. Rosenbaum, H. S., Deformation Twinning, p. 66, A. I. M. E. Met. Soc. Conf., Gordon and Breach, New York (1964).

44. Westlake, D. G., Deformation Twinning, p. 34, A. I. M. E. Met. Soc. Conf., Gordon and Breach, New York (1964).

45. Gilman, J. J., J. of Metals, 8, 1326 (1956).

46. Noggle, T. S., Rev. Sci. Instr., 24, 184 (1953).

47. Brandt, R. C., Adams, K. H., and Vreeland Jr., T., Cal. I. T. Res. Report, December (1961).

48. Elliott, H. A., Proc. Cambridge Phil. Soc., 44, 522 (1948).

49. Shield, R. T., Proc. Cambridge Phil. Soc., 47, 401 (1951).

50. Nye, J. F., Physical Properties of Crystals, p. 134, Oxford Press, London (1960).

51. Dean, W. R., Parson, H. W., and Sneddon, I. N., Proc. Cambridge Phil. Soc., 39, 5 (1943).